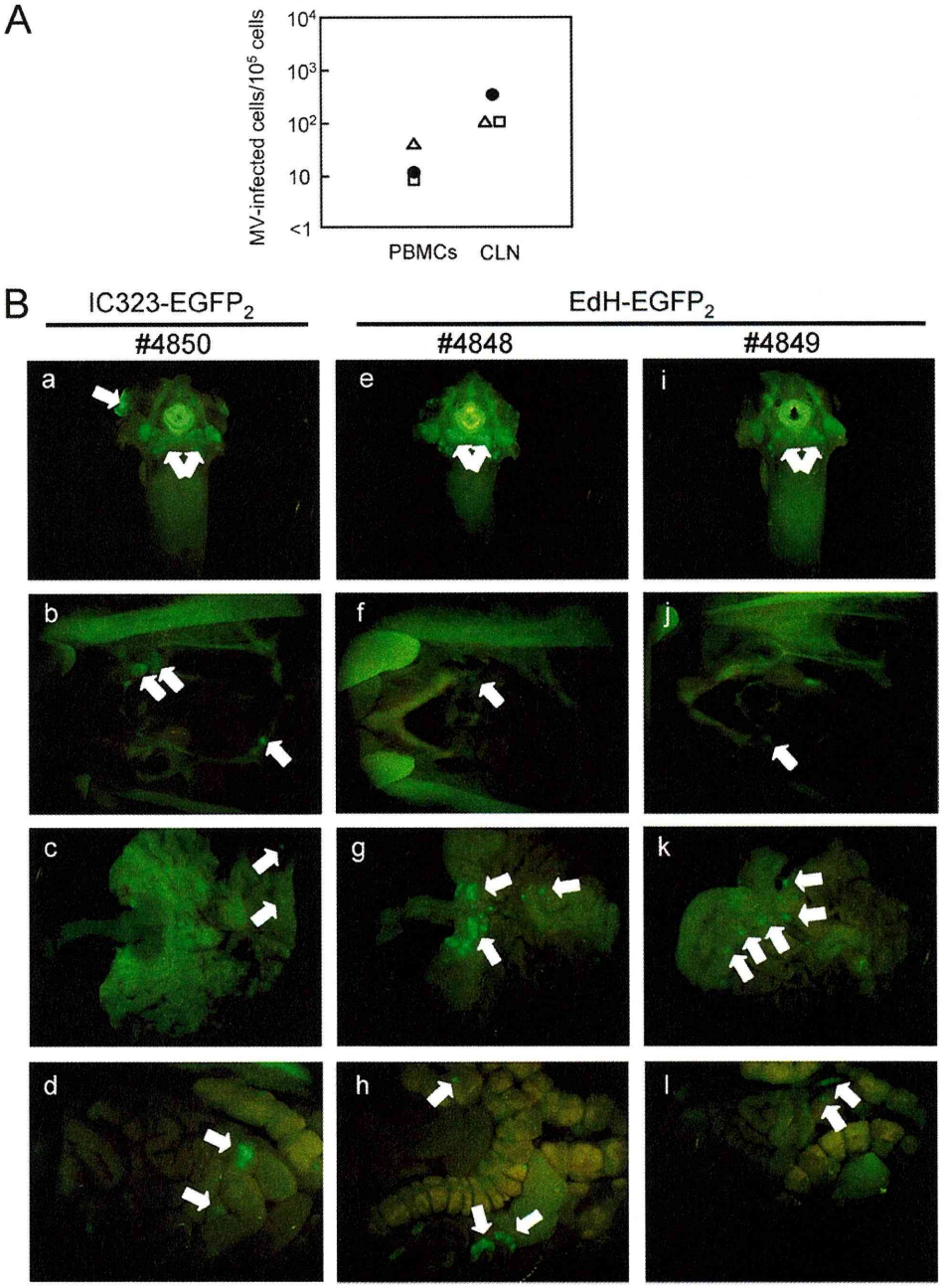

FIG 2 Detection of MV-infected cells in peripheral blood mononuclear cells (PBMCs) and cervical lymph nodes and EGFP expression in the tissues and organs of infected macaques. (A) One monkey (no. 4850) (closed circles) was infected with IC323-EGFP$_2$ and 2 monkeys (no. 4848 and 4849) (open triangles and open squares, respectively) were infected with EdH-EGFP$_2$. Single-cell suspensions (10^5/ml) from PBMCs and cervical lymph nodes (CLN) were divided into 2-fold serial dilutions, and then a 1-ml aliquot of each diluted single-cell suspension was inoculated into subconfluent B95a cells on 24-well cluster plates in duplicate. The number of MV-infected cells per 10^5 single-cell suspensions was then calculated. (B) At day 7, EGFP fluorescence in the tongue and tonsils (a, e, and i), cervical lymph nodes (b, f, and j), stomach (c, g, and k), and gut-associated lymph nodes (d, h, and l) was detected using a fluorescence microscope with a charge-coupled device (CCD) camera. Arrows indicate the MV-infected regions expressing EGFP.

monkeys. Prior to the infection of monkeys with IC323-EGFP$_2$ and EdH-EGFP$_2$, we examined the *in vitro* cell specificities of the two strains by using B95a and Vero cells and confirmed that EdH-EGFP$_2$ had the wider *in vitro* cell specificity (Fig. 1C). Then, one monkey (no. 4850) was inoculated with IC323-EGFP$_2$, and two monkeys (no. 4848 and 4849) were inoculated with EdH-EGFP$_2$. At day 7, viremia was observed in all 3 monkeys (Fig. 2A). Upon necropsy at day 7, nearly the same numbers of MV-infected cells were isolated from the cervical lymph nodes of the 3 monkeys (Fig. 2A). EGFP fluorescence was observed in many lymphoid tissues, including the cervical lymph nodes, tongue, tonsils, stomach, and gut-associated lymph nodes, in the 3 monkeys (Fig. 2B). No sig-

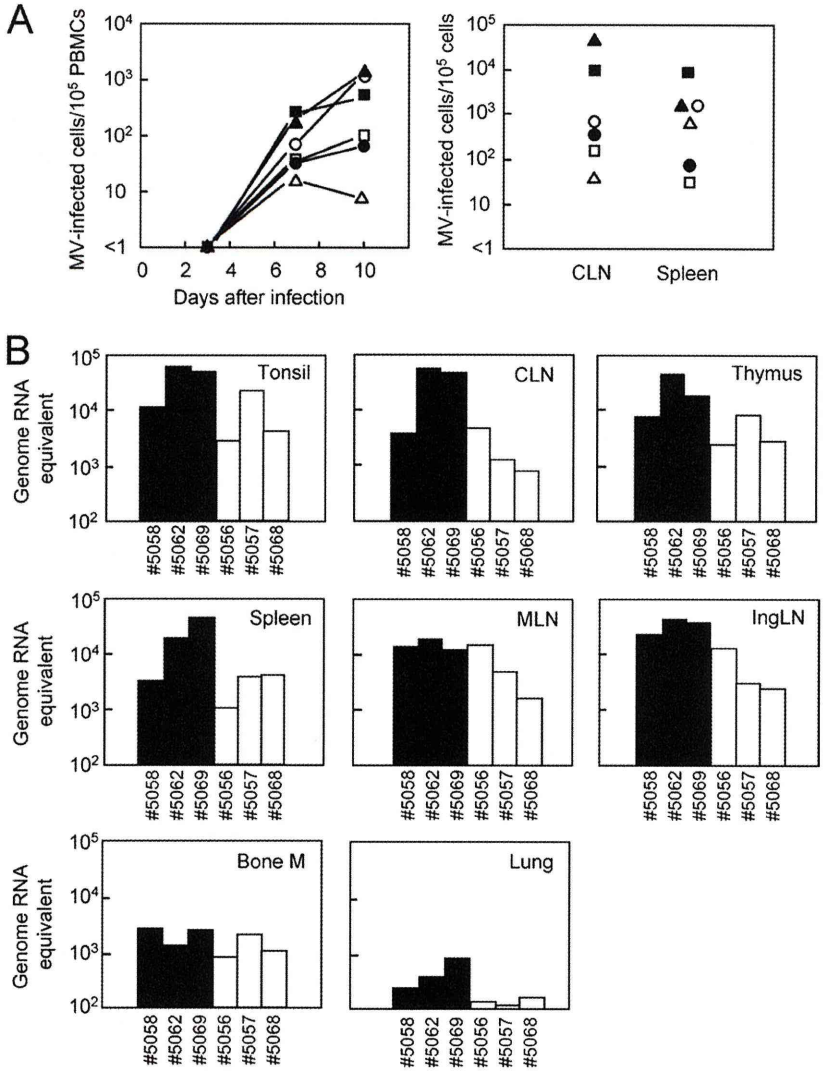

FIG 3 Detection of MV-infected cells and MV genome RNA. (A) Three monkeys (no. 5058, 5062, and 5069) (closed circles, closed triangles, and closed squares, respectively) were infected with IC323-EGFP$_2$, and 3 monkeys (no. 5056, 5057, and 5068) (open circles, open triangles, and open squares, respectively) were infected with EdH-EGFP$_2$. PBMCs were obtained at days 3, 7, and 10. CLN and spleens were obtained on day 10. Single-cell suspensions (10^5/ml) from PBMCs, CLN, and spleen were divided into 2-fold serial dilutions, and then a 1-ml aliquot of each diluted single-cell suspension was inoculated into subconfluent B95a cells on 24-well cluster plates in duplicate. The number of MV-infected cells per 10^5 single-cell suspensions was then calculated. (B) MV genome RNA was detected by real-time reverse transcription-PCR on total RNA isolated from tonsils, CLN, thymus, spleens, mesenteric lymph nodes (MLN), inguinal lymph nodes (IngLN), bone marrow (bone M), and lungs. Three monkeys (no. 5058, 5062 and 5069) were infected with IC323-EGFP$_2$, and 3 monkeys (no. 5056, 5057, and 5068) were infected with EdH-EGFP$_2$. The results for the real-time RT-PCR were expressed as genome RNA equivalent to plasmid p(+)MV323-EGFP.

nificant difference in the distributions and intensities of EGFP fluorescence in the internal organs and tissues was observed among the 3 monkeys, indicating that the tropism of EdH-EGFP$_2$ was not expanded *in vivo*.

Growth of recombinant MV strains in cynomolgus monkeys. To assess whether these results could be confirmed, 6 monkeys were infected with IC323-EGFP$_2$ or EdH-EGFP$_2$. Three monkeys (no. 5058, 5062, and 5069) were inoculated with IC323-EGFP$_2$, and 3 monkeys (no. 5056, 5057, and 5068) were inoculated with EdH-EGFP$_2$. At day 7, viremia was detected in all 6 monkeys, and the number of infected cells was increased at day 10 in most monkeys (Fig. 3A, left). Upon necropsy at day 10, MV-infected cells were isolated from the cervical lymph nodes and spleens of the 6 monkeys (Fig. 3A, right). In monkeys infected with IC323-EGFP$_2$ a large number of the lymphocytes (up to 49%) of cervical lymph nodes were infected, whereas in monkeys infected with EdH-EGFP$_2$, a smaller number (0.040 to 0.77%) of the lymphocytes of cervical lymph nodes were infected (Fig. 3A, right). Similarly, in monkeys infected with IC323-EGFP$_2$, a large number of the lymphocytes (up to 8.2%) in the spleen were infected, whereas in monkeys infected with EdH-EGFP$_2$, a smaller number (0.032 to 1.5%) of the lymphocytes in cervical lymph nodes were infected (Fig. 3A, right). In all 6 monkeys infected with either IC323-EGFP$_2$ or EdH-EGFP$_2$, substantial amounts of MV genome RNA were detected in the tonsils, cervical lymph nodes, thymus, spleen, mesenteric lymph nodes, inguinal lymph nodes, bone marrow,

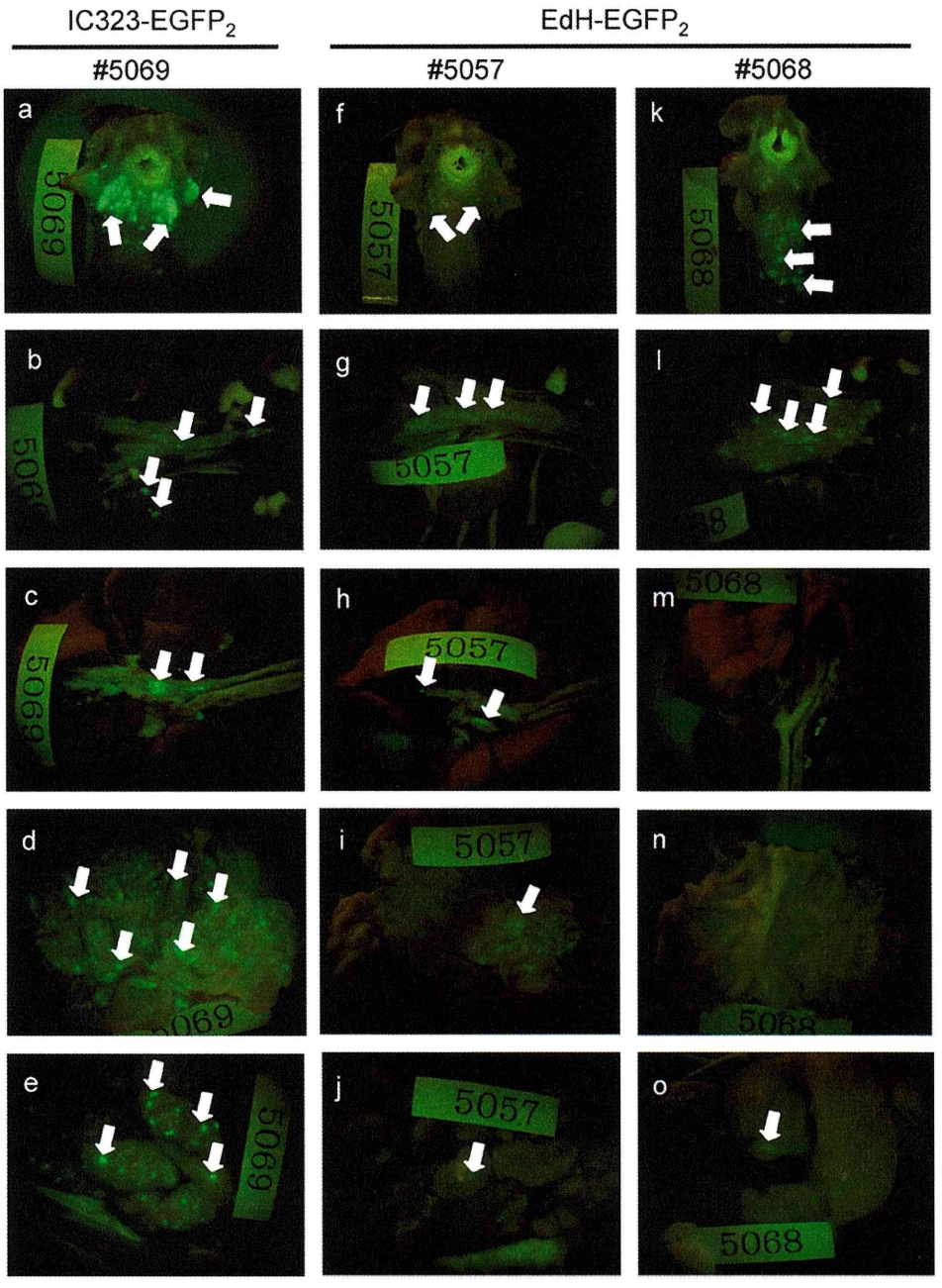

FIG 4 EGFP expression in tissues of monkeys after experimental infection with IC323-EGFP$_2$ and EdH-EGFP$_2$. At day 10, EGFP fluorescence in the tongue and tonsils (a, f, and k), thymus (b, g, and l), trachea and lung (c, h, and m), stomach (d, i, and n), and gut-associated lymph nodes (e, j, and o) of infected monkeys was detected using a fluorescence microscope with a CCD camera.

and lungs (Fig. 3B). We note that the amount of MV genome RNA in EdH-EGFP$_2$-infected monkeys was significantly lower than that in IC323-EGFP$_2$-infected monkeys, especially in lungs.

Macroscopic detection of EGFP fluorescence in organs and tissues. In all 6 monkeys infected by IC323-EGFP$_2$ or EdH-EGFP$_2$, EGFP fluorescence was macroscopically detected in many lymphoid organs and tissues, including the tongue and tonsils, thymus, trachea and lungs, stomach, and gut-associated lymph nodes, upon necropsy at day 10 (Fig. 4). No difference in the distribution of EGFP fluorescence in the internal organs and tissues was observed between monkeys infected with IC323-EGFP$_2$ or EdH-EGFP$_2$, confirming that tropism of EdH-EGFP$_2$ is not expanded in macaques. However, the intensity of EGFP fluorescence in the internal organs and tissues of EdH-EGFP$_2$-infected monkeys was significantly weaker than that in IC323-EGFP$_2$-infected monkeys.

Histopathological and immunohistochemical analyses. To further examine the tissue and organ tropism of IC323-EGFP$_2$ and EdH-EGFP$_2$, we performed histopathological and immunohistochemical analyses of fixed specimens. In bronchioles, we histo-

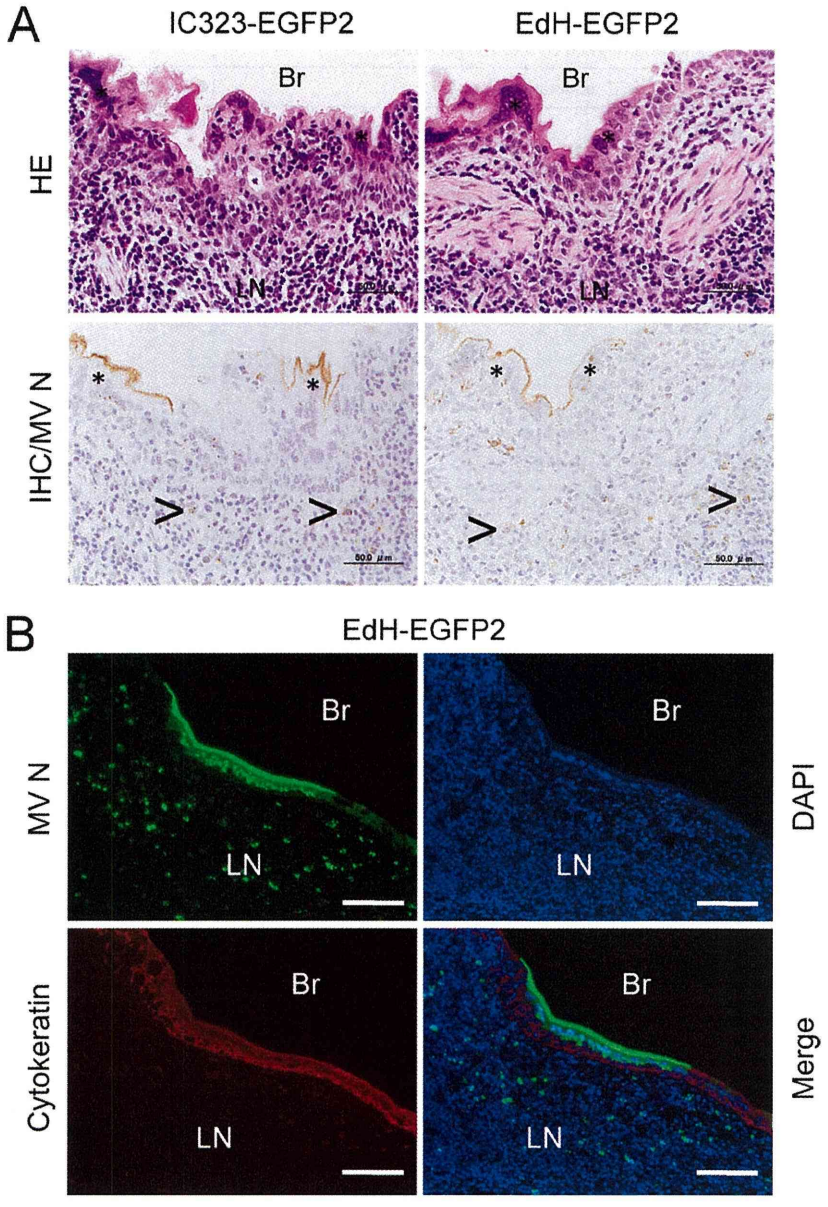

FIG 5 Histopathological and immunohistochemical analyses. (A) Bronchiole sections obtained from monkeys infected with IC323-EGFP$_2$ or EdH-EGFP$_2$ were examined by hematoxylin and eosin staining and immunohistochemistry. Giant-cell formation (*) and lymphoid filtrates were seen in the epithelial layer of the bronchiole. MV nucleocapsid (N) antigen (light brown) was detected in the cytoplasm and nucleus in the giant cells and in the cytoplasm of the lymphocytes (arrows) of lymphatic nodules under the epithelial layer by immunohistochemical analysis (IHC). (B) The bronchiole area obtained from a monkey infected with EdH-EGFP$_2$ was investigated by double immunofluorescence staining. Tissue sections were stained with antiserum against the MV N antigen and mouse monoclonal antibody against cytokeratin. DAPI was used to identify nuclei. Br, bronchiole; LN, lymphatic nodule. Bars, 50 μm (A) and 100 μm (B).

pathologically observed bronchiolitis and giant cells with eosinophilic inclusion bodies in monkeys infected with both IC323-EGFP$_2$ and EdH-EGFP$_2$, and MV N antigen was detected in both sections (Fig. 5A). Tissue sections obtained from the bronchiole area were double stained with anti-MV N and anticytokeratin antibodies, which clearly showed infection of EdH-EGFP$_2$ in the epithelial cells (Fig. 5B) as reported for wild-type MV (3, 20), possibly through a nectin-4-mediated pathway (18, 20, 23, 31). Interestingly, the N protein was accumulated under the apical plasma membrane of the infected cells (Fig. 5B), suggesting an intracellular mechanism of transport of the N protein to the apical plasma membrane. The MV N antigen was detected in the lymphocytes of the spleen, mesenteric and cervical lymph nodes, thymus, salivary gland, tonsils, stomach, and jejunum (Table 1), as well as in epithelia of the lungs, bronchi, tonsils, and stomach, but not in the muscles of the heart and in the epithelia of the liver, kidney, skin, tonsils, and stomach of most monkeys. These data again indicated that tropism of EdH-EGFP$_2$ was not expanded in macaques.

Flow cytometric analysis. To examine the cell tropism of IC323-EGFP$_2$ and EdH-EGFP$_2$ in lymphocytes, EGFP expression in lymphocytes isolated from PBMCs and mesenteric lymph

TABLE 1 Detection of giant cells and measles virus nucleocapsid antigen in different tissues by immunohistochemistry

Organ	Tissue or cell type	Detection of giant cells or antigens after: IC323-EGFP$_2$ infection of monkey no.: 5058 Giant cells	5058 Viral antigens	5062 Giant cells	5062 Viral antigens	5069 Giant cells	5069 Viral antigens	EdH-EGFP$_2$ infection of monkey no.: 5056 Giant cells	5056 Viral antigens	5057 Giant cells	5057 Viral antigens	5068 Giant cells	5068 Viral antigens
Lung	Epithelium	+	+	+	+	+	+	+	+	+	+	+	+
Bronchus	Epithelium	+	+	+	+	+	+	+	−	+	+	+	+
Heart	Muscle	−	−	−	−	−	−	−	−	−	−	−	−
Liver	Epithelium	−	−	−	+	−	−	−	−	−	−	−	−
Kidney	Epithelium	−	−	+	+	−	−	−	−	−	+	−	−
Skin	Epithelium	−	−	+	+	−	−	−	−	−	−	+	+
Spleen	Lymphocyte	+	+	+	+	+	+	+	+	+	+	−	−
Mesenteric lymph node	Lymphocyte	+	+	+	+	+	+	+	+	+	+	+	+
Cervical lymph node	Lymphocyte	+	+	+	+	+	+	+	+	+	+	+	+
Thymus	Lymphocyte	+	+	+	+	+	+	+	+	+	+	+	+
Salivary gland	Lymphocyte	−	−	−	+	−	+	−	+	−	+	−	+
Tonsil	Epithelium	NE[a]	NE	+	+	+	+	+	+	NE	NE	+	+
	Lymphocyte	NE	NE	+	+	+	+	+	+	NE	NE	+	+
Stomach	Epithelium	−	−	+	+	+	+	+	+	−	−	+	+
	Lymphocyte	−	+	−	+	−	+	−	+	−	+	−	+
Pancreas	Epithelium	−	−	−	−	−	−	−	−	−	−	−	−
Jejunum	Lymphocyte	−	+	−	+	−	+	−	+	−	+	−	+

[a] NE, not examined.

nodes was analyzed by flow cytometry. A total of 0.90% and 8.59% of B lymphocytes in PBMCs and MLNs, respectively, and 0.90% and 3.90% of T lymphocytes in PBMCs and MLNs, respectively, were infected with IC323-EGFP$_2$ (Fig. 6). Lymphocytes expressing SLAM were infected with IC323-EGFP$_2$, as previously reported (3). Similarly, 0.44 to 0.53% and 1.06 to 2.23% of B lymphocytes in PBMCs and MLNs, respectively, and 0.42 to 0.68% and 0.70 to 1.44% of T lymphocytes in PBMCs and MLNs, respectively, were infected with EdH-EGFP$_2$ (Fig. 6). Lymphocytes expressing SLAM were also infected with EdH-EGFP$_2$. These results indicated that tropism of EdH-EGFP$_2$ was not expanded in lymphocytes of macaques. Interestingly, the number and intensity of EGFP-expressing cells in lymphocytes of EdH-EGFP$_2$-infected monkeys were significantly lower than those in of IC323-EGFP$_2$-infected monkeys.

Cytokine production by infected monkeys. To investigate whether the differences in growth of IC323-EGFP$_2$ and EdH-EGFP$_2$ in monkeys were associated with altered host responses to infection, we measured cytokine and chemokine levels in plasma samples from infected monkeys. The cytokines selected for analysis were IL-12, IFN-γ, IL-2, IL-4, IL-5, and IL-17 (Th1/Th2 balance) and the IL-6, TNF-α, IL-1β, and MCP-1 (inflammatory response).

With Th1-type cytokines, we found that plasma levels of IL-12 were high for 3 (no. 5056, 5057, and 5062) out of 6 monkeys at day 0, were slightly elevated at day 3, and then declined by day 7 (Fig. 7). The plasma levels of IL-12 for the 3 other monkeys (no. 5058, 5068, and 5069) were low throughout the experiment. Irrespective of the plasma levels of IL-12, the plasma levels of IFN-γ were elevated in all 6 monkeys. The increase in plasma levels of IL-2 was marginal by day 10 for 5 monkeys. For inflammatory cytokines, the plasma level of MCP-1 was markedly elevated for all monkeys. IL-4, IL-17, and IL-1β were not detected throughout the experiment. Other cytokines (IL-5, IL-6, and TNF-α) were not consistently detected (data not shown).

Taking the results together, there were no significant differences in the cytokine production profiles of the monkeys infected with IC323-EGFP$_2$ or EdH-EGFP$_2$, and similar Th1-type and inflammatory responses against acute MV infection occurred in monkeys infected with IC323-EGFP$_2$ or EdH-EGFP$_2$.

DISCUSSION

In this study, we compared the cell specificities and tropisms of the wild-type strains of MV bearing the H protein of the Edmonston vaccine strain with those of the wild-type MV strains. Although EdH-EGFP showed wider cell specificity in cell lines and primary cell cultures (Fig. 1B), the tissue and organ tropism of EdH-EGFP$_2$ was not altered in all 5 infected macaques (Fig. 2 and 4 and Table 1). Since CD46 is ubiquitously expressed in human and monkey cells, EdH-EGFP$_2$ could infect all cells in macaques. However, widespread infection of EdH-EGFP$_2$ in tissues and organs was not observed. This result is not surprising because it was reported that only the lymph nodes and spleen of monkeys were infected with MV vaccine strains (39). Furthermore, it was recently reported that CD11c-positive myeloid cells, such as alveolar macrophages and dendritic cells in lungs of monkeys, were infected with an EGFP-expressing recombinant Edmonston strain of MV via an aerosol route (5). This result is consistent with our findings in that the CD46-using Edmonston vaccine strain does not cause widespread infection in the lungs of monkeys, although there is a possibility that the infection by the Edmonston strain in lungs may be restricted due to mutations in the N and P/C/V genes, which are most important in combating the innate immune system.

One possible explanation for the limited infection of EdH-EGFP$_2$ in macaques is the expression level of CD46. Anderson et al. reported that at low CD46 density, infection with the MV vac-

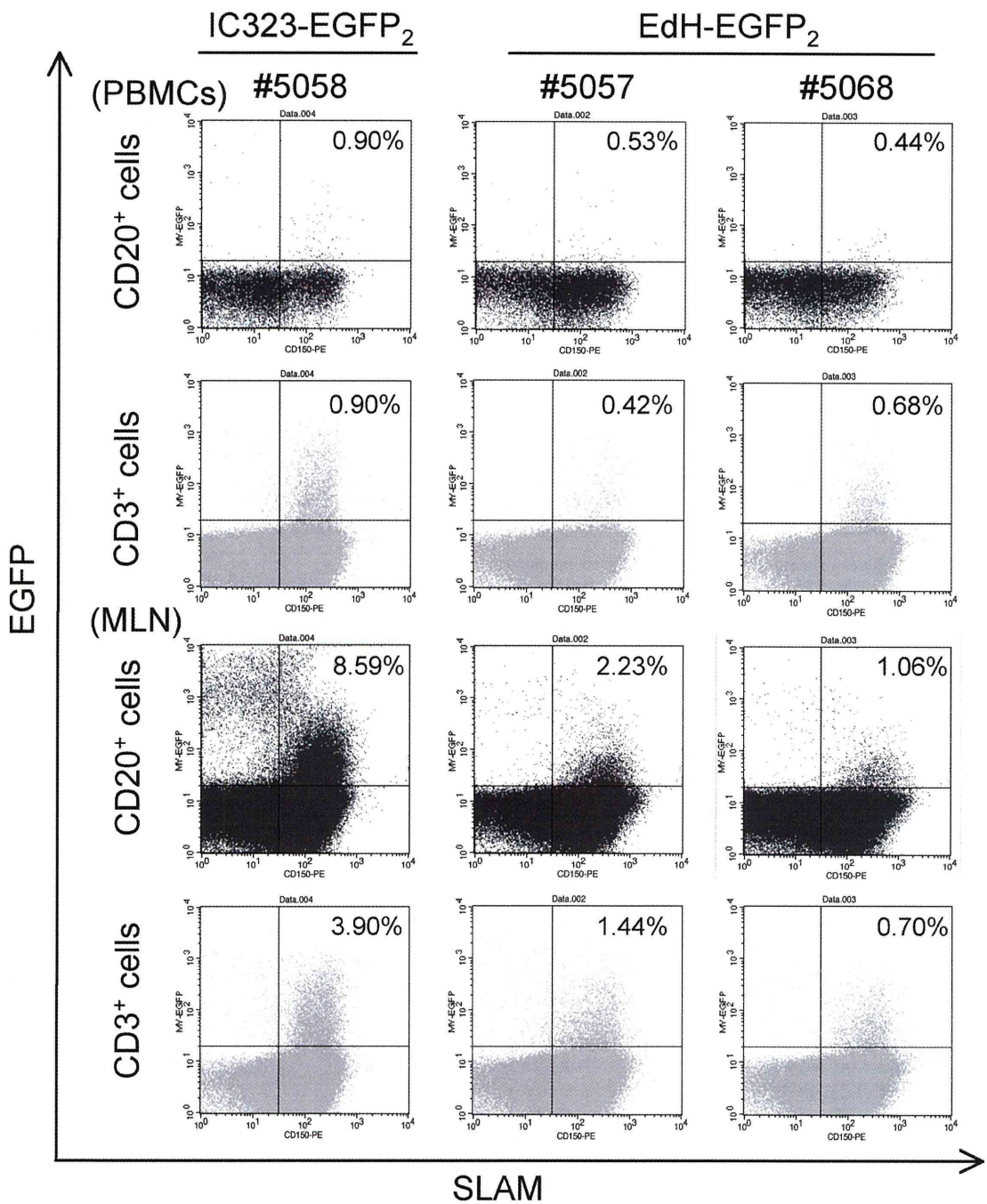

FIG 6 EGFP-positive cells in lymphocyte subpopulations of PBMCs and mesenteric lymph nodes from infected monkeys. Cryopreserved PBMCs and mesenteric lymph nodes (MLN) of monkeys infected with IC323-EGFP$_2$ (no. 5058) or EdH-EGFP$_2$ (no. 5057 and 5068) were stained with monoclonal antibodies against CD3, CD20, and CD150 (signaling lymphocyte activation molecule [SLAM]) and analyzed with a FACSCalibur instrument. Results are shown as dot plots, with SLAM expression on the *x* axis and EGFP expression on the *y* axis. EGFP expression in CD20$^+$ B lymphocytes and CD3$^+$ T lymphocytes is shown. CD46 expression in lymphocytes of PBMCs of monkeys infected with EdH-EGFP$_2$ (no. 5057 and 5068) was detected with monoclonal antibody against CD46 and isotype control antibody.

cine strain occurs but subsequent cell-to-cell fusion does not (1). If the expression levels of CD46 are low in cells in the tissues, EdH-EGFP$_2$ may infect those cells, but subsequent cell-to-cell fusion may not occur. In primary cell cultures, gene expression profiles often change when tissue cells are cultured *in vitro*. Thus, it is likely that the CD46 expression levels of primary cell cultures are high enough for infection with EdH-EGFP. We are now examining the expression levels of CD46 in cell lines and primary cell cultures and in tissues of cynomolgus monkeys. Another possible explanation for the limited infection of EdH-EGFP$_2$ in macaque tissues is the inefficient replication of MV due to interferons. Yoshikawa et al. reported that primate kidney cells rapidly lose

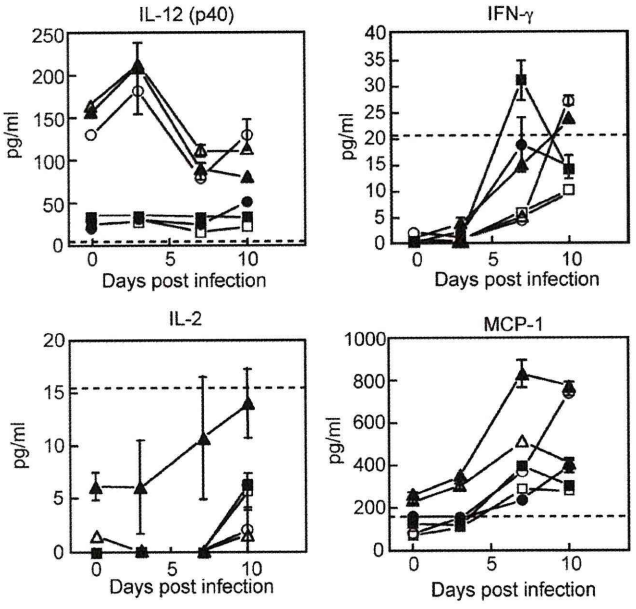

FIG 7 Detection of cytokines in plasma samples from infected monkeys. Three monkeys (no. 5058, 5062, and 5069) (closed circles, closed triangles, and closed squares, respectively) were infected with IC323-EGFP$_2$. Three other monkeys (no. 5056, 5057, and 5068) (open circles, open triangles, and open squares, respectively) were infected with EdH-EGFP$_2$. Plasma was obtained at days 0, 3, 7, and 10. Cytokine levels in the plasma were measured with a Luminex 200 instrument using a Milliplex nonhuman primate cytokine/chemokine kit. The physiological upper concentration ranges detected in human plasma are indicated by dotted lines.

interferon-inducing activity and permit poliovirus replication when the cells are cultured *in vitro* (40). MV replication in monkey tissues may be inhibited by interferon, whereas MV replication in primary cell cultures can occur due to the lack of interferon-inducing activity.

Flow cytometric analysis showed that lymphocytes expressing SLAM were infected with both IC323-EGFP$_2$ and EdH-EGFP$_2$ (Fig. 6). It is known that stimulated lymphocytes can be efficiently infected with MV and that SLAM is highly expressed in stimulated lymphocytes (11). Thus, the activation status of lymphocytes may be important for infection with MV, and infection of unstimulated lymphocytes with EdH-EGFP$_2$ by the CD46-mediated pathway would not result in efficient MV replication. As a result, lymphocytes expressing SLAM may appear to be equally infected with both strains. Recently, two groups revealed that both SLAM and CD46 are required for stable transduction of resting human lymphocytes with lentiviral vectors pseudotyped with the vaccine MV F and H proteins (8, 42). Thus, another possibility is that SLAM binding in addition to CD46 binding may be required for efficient infection of lymphocytes with EdH-EGFP$_2$. SLAM binding and subsequent signaling (8, 42) may be important for efficient MV infection.

A previous study in which monkeys were infected with pathogenic and Edmonston vaccine strains via an aerosol route showed that only the pathogenic strain caused massive infection in lymphoid tissues (5). We also infected monkeys with IC323-EGFP$_2$ and EdH-EGFP$_2$ via the aerosol route, and we found that both strains caused massive infection in lymphoid tissues (Fig. 3). This result indicated that the Edmonston H protein does not influence the extent of infection in lymphoid tissues. Proteins other than the H protein, possibly viral polymerase proteins (30), may regulate MV replication in lymphoid tissues.

Suppression of the production of IL-12 during measles was proposed (10). We found that the initial level of IL-12 was high for 3 monkeys (no. 5056, 5057, and 5062) but low for 3 other monkeys (no. 5058, 5068, and 5069) (Fig. 7). We do not have an explanation for this difference. However, our results indicated that the IL-12 levels were not significantly induced at early time points during MV infection. This result may be consistent with a previous observation of suppressed serum levels of IL-12 during MV infection in rhesus macaques (13, 26). Interestingly, Th1-type cytokines (IFN-γ and IL-2) were induced in all monkeys irrespective of the IL-12 level. The induction of IFN-γ in plasma at early time points is consistent with that in previous studies of human measles (10, 19, 24, 41). A previous study showed no significant induction of IL-2, IL-12, and IFN-γ in monkeys infected with wild-type MV (4). However, in that experiment the induction of IL-2, IL-12, and IFN-γ was measured by quantitating their mRNAs by real-time RT-PCR using RNA extracted from PBMCs. Real-time RT-PCR data may not coincide with the actual amounts of cytokines in plasma.

In summary, the current study showed that the H protein of the Edmonston vaccine strain alters the cell specificity of wild-type MV *in vitro* but not the tropism in macaques. SLAM$^+$ cells were main target for both IC323-EGFP$_2$ and EdH-EGFP$_2$ in macaques. In addition, it is suggested that the Edmonston vaccine H protein attenuates MV growth *in vivo*, especially at a later stage. It has long been proposed that the vaccine H protein attenuates the virus growth *in vivo* by several mechanisms (e.g., CD46-mediated signaling in infected cells or downregulation of CD46 in infected cells and subsequent complement-mediated cell lysis) (14). It will be interesting to examine the type I interferon production and the downregulation of CD46 in MV-infected cells in monkeys infected with EdH-EGFP$_2$ or MV vaccine strains.

ACKNOWLEDGMENTS

We thank Y. Yanagi and M. Takeda for providing plasmids and cells, B. Moss for vaccinia virus vTF7-3, N. Kimura for primary monkey astroglial cells, A. Harashima, M. Fujino, H. Sato, Y. Saito, A. Wakutsu, K. Kato, and T. Nishie for excellent technical support, and Y. Yasutomi, K. Terao, A. Yamada, T. Sata, H. Hasegawa, and K. Komase for valuable discussions and continuous support. We also thank K. Ho for critical readings and valuable comments.

This work was supported in part by a grant-in-aid (no. 21022006 and 23659227) from the Ministry of Education, Culture, Sports, Science and Technology of Japan.

REFERENCES

1. **Anderson BD, Nakamura T, Russell SJ, Peng K-W.** 2004. High CD46 receptor density determines preferential killing of tumor cells by oncolytic measles virus. Cancer Res. **64**:4919–4926.
2. **Auwaerter PG, et al.** 1999. Measles virus infection in rhesus macaques: altered immune responses and comparison of the virulence of six different virus strains. J. Infect. Dis. **180**:950–958.
3. **de Swart RL, et al.** 2007. Predominant infection of CD150+ lymphocytes and dendritic cells during measles virus infection of macaques. PLoS Pathog. **3**:e178.
4. **Devaux P, Hodge G, McChesney MB, Cattaneo R.** 2008. Attenuation of V- or C-defective measles viruses: infection control by the inflammatory and interferon responses of rhesus monkeys. J. Virol. **82**:5359–5367.
5. **de Vries RD, et al.** 2010. In vitro tropism of attenuated and pathogenic measles virus expressing green fluorescent protein in macaques. J. Virol. **84**:4714–4724.

6. **Dorig RE, Marcil A, Chopra A, Richardson CD.** 1993. The human CD46 molecule is a receptor for measles virus (Edmonston strain). Cell **75**:295–305.
7. **Enders JF, Peebles TC.** 1954. Propagation in tissue cultures of cytopathic agents from patients with measles. Proc. Soc. Exp. Biol. Med. **86**:277–286.
8. **Frecha C, et al.** 2011. Measles virus glycoprotein-pseudotyped lentiviral vector-mediated gene transfer into quiescent lymphocytes requires binding to both SLAM and CD46 entry receptors. J. Virol. **85**:5975–5985.
9. **Fuerst TR, Niles EG, Studier FW, Moss B.** 1986. Eukaryotic transient-expression system based on recombinant vaccinia virus that synthesizes bacteriophage T7 RNA polymerase. Proc. Natl. Acad. Sci. U. S. A. **83**: 8122–8126.
10. **Griffin DE, Ward BJ, Jauregui E, Johnson RT, Vaisberg A.** 1990. Immune activation during measles: interferon-γ and neopterin in plasma and cerebrospinal fluid in complicated and uncomplicated disease. J. Infect. Dis. **161**:449–453.
11. **Griffin DE.** 2007. Measles virus, p 1551–1585. *In* Knipe DM, Howley PM, Griffin DE, Lamb RA, Martin MA, Roizman B, Straus SE (ed), Fields virology, 5th ed. Lippincott Williams & Wilkins, Philadelphia, PA.
12. **Hashimoto K, et al.** 2002. SLAM (CD150)-independent measles virus entry as revealed by recombinant virus expressing green fluorescent protein. J. Virol. **76**:6743–6749.
13. **Hoffman SJ, et al.** 2003. Vaccination of rhesus macaques with a recombinant measles virus expressing interleukin-12 alters humoral and cellular immune responses. J. Infect. Dis. **188**:1553–1561.
14. **Kemper C, Atkinson JP.** 2009. Measles virus and CD46. Curr. Top. Microbiol. Immunol. **329**:31–57.
15. **Kobune F, Sakata H, Sugiura A.** 1990. Marmoset lymphoblastoid cells as a sensitive host for isolation of measles virus. J. Virol. **64**:700–705.
16. **Kobune F, et al.** 1996. Nonhuman primate models of measles. Lab. Anim. Sci. **46**:315–320.
17. **Lamb RA, Parks GD.** 2007. *Paramyxoviridae*: the viruses and their replication, p 1449–1496. *In* Knipe DM, Howley PM, Griffin DE, Lamb RA, Martin MA, Roizman B, Straus SE (ed), Fields virology, 5th ed. Lippincott Williams & Wilkins, Philadelphia, PA.
18. **Leonard VHJ, et al.** 2008. Measles virus blind to its epithelial cell receptor remains virulent in rhesus monkeys but cannot cross the airway epithelium and is not shed. J. Clin. Invest. **118**:2448–2458.
19. **Moss WJ, Ryon JJ, Monze M, Griffin DE.** 2002. Differential regulation of interleukin (IL)-4, IL-5, and IL-10 during measles in Zambian children. J. Infect. Dis. **186**:879–887.
20. **Muhlebach MD, et al.** 2011. Adherens junction protein nectin-4 is the epithelial receptor for measles virus. Nature **480**:530–533.
21. **Naniche D, et al.** 1993. Human membrane cofactor protein (CD46) acts as a cellular receptor for measles virus. J. Virol. **67**:6025–6032.
22. **Navaratnarajah C, Leonard KVHJ, Cattaneo R.** 2009. Measles virus glycoprotein complex assembly, receptor attachment, and cell entry. Curr. Top. Microbiol. Immunol. **330**:59–76.
23. **Noyce RS, et al.** Tumor cell marker PVRL4 (nectin 4) is an epithelial cell receptor for measles virus. ProS Pahog. **7**:e1002240.
24. **Ohga S, Miyazaki C, Okada K, Akazawa K, Ueda K.** 1992. The inflammatory cytokines in measles: correlation between serum interferon-γ levels and lymphocyte subpopulations. Eur. J. Pediatr. **151**:492–496.
25. **Plumet S, Gerlier D.** 2005. Optimized SYBR green real-time PCR assay to quantify the absolute copy number of measles virus RNAs using gene specific primers. J. Virol. Methods **128**:79–87.
26. **Polack FP, Hoffman SJ, Moss WJ, Griffin DE.** 2002. Altered synthesis of interleukin-12 and type 1 and type 2 cytokines in rhesus macaques during measles and atypical measles. J. Infect. Dis. **185**:13–19.
27. **Rota JS, Wang ZD, Rota PA, Bellini WJ.** 1994. Comparison of sequences of the H, F, and N coding genes of measles virus vaccine strains. Virus Res. **31**:317–330.
28. **Tahara M, Takeda M, Seki F, Hashiguchi T, Yanagi Y.** 2007. Multiple amino acid substitutions in hemagglutinin are necessary for wild-type measles virus to acquire the ability to use receptor CD46 efficiently. J. Virol. **81**:2564–2572.
29. **Takeda M, et al.** 2005. Efficient rescue of measles virus from cloned cDNA using SLAM-expressing Chinese hamster ovary cells. Virus Res. **108**:161–165.
30. **Takeda M, et al.** 2008. Measles viruses possessing the polymerase protein genes of the Edmonston vaccine strain exhibit attenuated gene expression and growth in cultured cells and SLAM knock-in mice. J. Virol. **82**:11979–11984.
31. **Takeda M, et al.** 2007. A human lung carcinoma cell line supports efficient measles virus growth and syncytium formation via a SLAM- and CD46-independent mechanism. J. Virol. **81**:12091–12096.
32. **Takeda M, et al.** 2000. Recovery of pathogenic measles virus from cloned cDNA. J. Virol. **74**:6643–6647.
33. **Takeuchi K, Miyajima N, Kobune F, Tashiro M.** 2000. Comparative nucleotide sequence analyses of the entire genomes of B95a cell-isolated and Vero cell-isolated measles viruses from the same patient. Virus Genes **20**:253–257.
34. **Takeuchi K, et al.** 2005. Stringent requirement for the C protein of wild-type measles virus for growth in vitro and in macaques. J. Virol. **79**:7838–7844.
35. **Takeuchi K, et al.** 2002. Recombinant wild-type and Edmonston strain measles viruses bearing heterologous H proteins: role of H protein in cell fusion and host cell specificity. J. Virol. **76**:4891–4900.
36. **Tatsuo H, Ono N, Tanaka K, Yanagi Y.** 2000. SLAM (CDw150) is a cellular receptor for measles virus. Nature **406**:893–897.
37. **van Binnendijk RS, van der Heijden RW, van Amerongen G, Uytde-Haag FG, Osterhaus AD.** 1994. Viral replication and development of specific immunity in macaques after infection with different measles virus strains. J. Infect. Dis. **170**:443–448.
38. **von Messling V, Milosevic D, Cattaneo R.** 2004. Tropism illuminated: lymphocyte-based pathways blazed by lethal morbillivirus through the host immune system. Proc. Natl. Acad. Sci. U. S. A. **101**:14216–14221.
39. **Yamanouchi K, et al.** 1970. Giant cell formation in lymphoid tissue of monkeys inoculated with various strains of measles virus. Jpn. J. Med. Sci. Biol. **23**:131–145.
40. **Yoshikawa T, et al.** 2006. Role of the alpha/beta interferon response in the acquisition of susceptibility to poliovirus by kidney cells in culture. J. Virol. **80**:4313–4325.
41. **Yu X, et al.** 2008. Measles virus infection in adults induces production of IL-10 and is associated with increased CD4+CD25+ regulatory T cells. J. Immunol. **181**:7356–7366.
42. **Zhou Q, Schneider IC, Gallet M, Kneissl S, Buchholz CJ.** 2011. Resting lymphocyte transduction with measles virus glycoprotein pseudotyped lentiviral vectors relies on CD46 and SLAM. Virology **413**:149–152.

JOURNAL OF VIROLOGY, July 2011, p. 6197–6204 Vol. 85, No. 13
0022-538X/11/$12.00 doi:10.1128/JVI.00277-11

Replication-Coupled and Host Factor-Mediated Encapsidation of the Influenza Virus Genome by Viral Nucleoprotein▽

Atsushi Kawaguchi,[1,2] Fumitaka Momose,[2] and Kyosuke Nagata[1]*

Department of Infection Biology, Graduate School of Comprehensive Human Sciences, University of Tsukuba, 1-1-1 Tennodai, Tsukuba 305-8575, Japan,[1] and Kitasato Institute for Life Sciences, Kitasato University, 5-9-1 Shirokane, Minato-ku, Tokyo 108-8641, Japan[2]

Received 7 February 2011/Accepted 11 April 2011

The influenza virus RNA-dependent RNA polymerase is capable of initiating replication but mainly catalyzes abortive RNA synthesis in the absence of viral and host regulatory factors. Previously, we reported that IREF-1/minichromosome maintenance (MCM) complex stimulates a *de novo* initiated replication reaction by stabilizing an initiated replication complex through scaffolding between the viral polymerase and nascent cRNA to which MCM binds. In addition, several lines of genetic and biochemical evidence suggest that viral nucleoprotein (NP) is involved in successful replication. Here, using cell-free systems, we have shown the precise stimulatory mechanism of virus genome replication by NP. Stepwise cell-free replication reactions revealed that exogenously added NP free of RNA activates the viral polymerase during promoter escape while it is incapable of encapsidating the nascent cRNA. However, we found that a previously identified cellular protein, RAF-2p48/NPI-5/UAP56, facilitates replication reaction-coupled encapsidation as an NP molecular chaperone. These findings demonstrate that replication of the virus genome is followed by its encapsidation by NP in collaboration with its chaperone.

The genome of influenza type A viruses consists of eight-segmented and single-stranded RNAs of negative polarity. Transcription from the viral RNA (vRNA) genome is initiated using the oligonucleotide containing the cap-1 structure from cellular pre-mRNAs as a primer, whereas genome replication is primer independent and generates full-length vRNA through cRNA (full-sized complementary copy of vRNA) (reviewed in reference 17). Generally, each viral DNA or RNA genome is not present as a naked form but as a complex with viral basic proteins. The influenza virus genome exists as a ribonucleoprotein (termed vRNP) complex with nucleoprotein (NP), one of the basic viral proteins, and viral RNA-dependent RNA polymerases consisting of three subunits (PB1, PB2, and PA). NP binds single-stranded RNA without sequence specificity and is required for maintaining the RNA template in an ordered conformation suitable for viral RNA synthesis and packaging into virions (6, 23, 34). In the case of *Mononegavirales*, nonsegmented and negative-stranded RNA viruses, it is proposed that the nucleocapsid (N) protein forms a trimeric complex with the viral RNA polymerase large (L) protein and phosphoprotein (P) to form a replicase complex to produce the progeny viral genome with concomitant encapsidation of nascent RNA by N protein and that encapsidation is mediated by the chaperone activity of P protein (2, 7, 14, 24). In the case of influenza virus, it is also postulated that NP might regulate the viral polymerase function and encapsidate the virus genome through its interaction with PB1 and/or PB2 (1, 23). Genetic analyses suggest that NP participates in the replication process (15). Recently, it was also shown that NP that is saturated with single-stranded DNA (ssDNA), resulting in the lack of RNA binding activity, stimulates virus genome replication from a model template without primer (18). It is possible that NP stimulates virus genome replication through interaction with the viral polymerase in an RNA binding activity-independent manner. Moreover, the *in vitro* cRNA synthesis using infected cell extracts as an enzyme source depends on a supply of NP free of RNA (27). This finding has been interpreted as indicating that NP prevents the premature termination of RNA synthesis, possibly by binding to nascent RNA chains, that is, encapsidating them. Based on these observations, it could be hypothesized that NP facilitates virus genome replication by both RNA binding- and viral polymerase binding-dependent mechanisms. It is proposed that encapsidation is initiated by successive targeting of exogenous NP monomer to a replicating RNA through the interaction between NP and the viral polymerase, which is distinct from the replicative enzyme bound to the 5′ end of nascent RNA (1, 8, 11, 22), and then additional NP molecules are subsequently recruited by the NP-NP oligomerization (3, 23). It is also reported that nascent cRNA is degraded by host cellular nucleases unless it is stabilized by newly synthesized viral RNA polymerases and NP (33). However, the precise molecular mechanisms involved in virus genome replication and encapsidation by NP are yet unclear.

The cRNA synthesis occurs from incoming vRNA in infected cells, but vRNP complexes isolated from virions by themselves hardly synthesize cRNA (9). Thus, it was reasonable to examine whether a host factor(s) and/or a viral factor(s) is required for the replication process. We reconstituted a cell-free virus genome replication system with virion-associated vRNP and nuclear extracts prepared from uninfected HeLa cells (9). Using biochemical fractionation and complementation assays, we identified influenza virus replication factor 1 (IREF-1) that enabled the viral polymerase to synthesize

* Corresponding author. Mailing address: Department of Infection Biology, Graduate School of Comprehensive Human Sciences, University of Tsukuba, 1-1-1 Tennodai, Tsukuba 305-8575, Japan. Phone and fax: 81 29 853 3233. E-mail: knagata@md.tsukuba.ac.jp.

▽ Published ahead of print on 20 April 2011.

full-sized cRNA. Otherwise, the viral RNA polymerase produces mainly abortive short RNA chains in the absence of IREF-1. IREF-1 was found to be identical with a minichromosome maintenance (MCM) heterohexamer complex. IREF-1/MCM stabilizes replicating polymerase complexes by promoting the interaction between the nascent cRNA and the PA subunit.

Here, we examined the molecular function of NP in influenza virus genome replication using a previously established cell-free virus genome replication system and virion-associated vRNP. Exogenously added NP free of RNA stimulated virus genome replication with MCM in an additive manner. Further, we found that NP activates the viral polymerase during its transition from initiation to elongation to synthesize the unprimed full-length cRNA, but NP by itself is incapable of encapsidating the nascent cRNA. However, we found that RAF-2p48/NPI-5/UAP56/BAT1, which was identified as a host factor for activation of viral RNA synthesis (16), is required for the encapsidation of nascent cRNA with exogenously added NP free of RNA and for the stimulation of the elongation process of virus genome replication. We observed that the level of the virus genome replication was decreased in infected cells when the expression of the RAF-2p48/UAP56 gene was knocked down by small interfering RNA (siRNA)-mediated gene silencing. Based on these observations, we propose an NP- and host factor-dependent mechanism of virus genome encapsidation in concert with its replication.

MATERIALS AND METHODS

Biological materials. vRNP was prepared from purified influenza A/Puerto Rico/8/34 virus as previously described (28). For the expression of His-tagged NP (His-NP), we cloned the open reading frame (ORF) corresponding to the NP gene into pET14b. Rabbit polyclonal antibody against NP was generated by immunization of a 2-month-old female rabbit with His-NP protein. HeLa cells were grown in Dulbecco's modified Eagle's medium (DMEM) supplemented with 10% fetal bovine serum.

Preparation of recombinant proteins. His-tagged recombinant proteins were prepared and purified according to the manufacturer's protocol. In addition, to remove the bacterial RNA possibly bound to NP, we treated recombinant proteins with RNase A before purification and washed them with a buffer containing 1 M NaCl. Recombinant RAF-2p48/UAP56 was prepared from glutathione *S*-transferase (GST)-tagged RAF-2p48/UAP56 by PreScission protease (GE Health Care) digestion. Purified proteins were stored in a buffer containing 50 mM HEPES-NaOH (pH 7.9), 300 mM KCl, 20% glycerol, and 1 mM dithiothreitol (DTT) at −80°C until use. Recombinant MCM complex was prepared as previously described (9). These purified recombinant proteins were separated by SDS-PAGE and visualized by staining with Coomassie brilliant blue in Fig. 1A.

Cell-free virus genome replication system. Cell-free virus genome replication was carried out at 30°C for 90 min in a final volume of 25 μl containing 50 mM HEPES-NaOH (pH 7.9), 5 mM $MgCl_2$, 50 mM KCl, 1.5 mM dithiothreitol, 500 μM each ATP, CTP, and UTP, 25 μM GTP, 5 μCi of [α-^{32}P]GTP (3,000 Ci/mmol), 8 U of RNase inhibitor, and vRNP (10 ng of NP equivalents) in the presence or absence of purified proteins. RNA products were purified, subjected to 4% PAGE in the presence of 8 M urea, and visualized by autoradiography. For limited elongation assays, RNA synthesis was performed with vRNP (150 ng of NP equivalents) in the absence of UTP, and RNA products were separated by 15% PAGE containing 8 M urea. To address the encapsidation of nascent cRNA with NP, RNA synthesis was carried out by following the standard protocol described above except that 0.3 μM UTP, 250 μM each ATP, CTP, and GTP, and 10 μCi of [α-^{32}P]UTP (3,000 Ci/mmol) were used in a final volume of 200 μl. The coprecipitated RNA products with NP or MCM were separated through 10% PAGE containing 8 M urea.

Gene silencing mediated by siRNA. An siRNA against the RAF-2p48/UAP56 gene corresponding to its open reading frame (5′-AGUACUACGUGAAACU GAAGGACAA-3′) and control double-stranded RNA (dsRNA) targeting none of the cellular mRNAs were designed and synthesized by iGENE Therapeutics Inc. HeLa cells (1×10^5 cells) were transfected with 40 pmol of siRNA using Lipofectamine 2000 (Invitrogen) according to the manufacturer's protocol. At 48 h posttransfection, the cells were infected with influenza A/PR/8/34 at a multiplicity of infection (MOI) of 10 in the absence or presence of 100 μg/ml of cycloheximide (CHX). The RAF-2p48/UAP56 knockdown cells were also transfected with viral protein expression plasmids encoding PB1, PB2, PA, and NP and pHH21-vNS-Luc reporter plasmid to reconstitute a model viral replicon (19, 30). This reporter plasmid carries the luciferase (Luc) gene in reverse orientation sandwiched between 23-nucleotide (nt)-long 5′-terminal and 26-nucleotide-long 3′-terminal promoter sequences of the influenza virus segment 8, which is placed under the control of the human polymerase I (Pol I) promoter.

Indirect immunofluorescence assay. HeLa cells on coverslips were fixed with 4% paraformaldehyde in phosphate-buffered saline (PBS). The cells were permeabilized in 0.5% Triton X-100 and incubated in PBS containing 1% bovine serum albumin (BSA). The coverslips were incubated with anti-RAF-2p48/UAP56 rabbit polyclonal antibody (16) for 1 h. After a washing step with 0.1% Tween 20 in PBS, coverslips were incubated with Alexa Fluor 568-conjugated anti-rabbit IgG (Invitrogen) for 1 h. Images were acquired under the same exposure time by a fluorescence microscope system (Axiovision; Carl Zeiss).

Primer extension assay. Total RNAs isolated from control and RAF-2p48/UAP56 knockdown cells at 0, 3, 6, and 9 h postinfection (hpi) were subjected to reverse transcription at 42°C for 1 h with primers specific for segment 5 vRNA (5′-GGGAATACAGAGGGGAGAA-3′) corresponding to the NP cDNA between nucleotide sequence positions 1336 and 1354, segment 5 m/cRNA (5′-G ATTTCAGTGGCATTCTGGC-3′) complementary to the NP cDNA between nucleotide sequence positions 101 and 120, and 5S rRNA (5′-GGGGTACCTT CGAAAGCCTACAGCACCCGGTA-3′), which were labeled at their 5′ ends with [γ-^{32}P]ATP and T4 polynucleotide kinase (Toyobo). The products purified with phenol-chloroform extraction and ethanol precipitation were separated through 6% polyacrylamide gel containing 7 M urea and visualized by autoradiography.

Real-time quantitative PCR. Total RNAs isolated from control and RAF-2p48/UAP56 knockdown cells at 12 h posttransfection for construction of the model viral replicon were subjected to reverse transcription with primers to determine the level of vRNA (5′-TCCATCACGGTTTTGGAATGTTTACTA CAC-3′, which corresponds to the luciferase coding region between nucleotide sequence positions 728 and 757), cRNA (5′-AGTAGAAACAAGGGTGTTTT TTAGTA-3′, which is complementary to the 3′ portion of the segment 8 cRNA), and viral mRNA [oligo$(dT)_{20}$ for poly(A) tail] synthesized from the reconstituted model viral replicon. The synthesized single-stranded cDNAs were subjected to real-time quantitative PCR analysis (Thermal Cycler Dice Real Time System TP800; TaKaRa) with two specific primers, 5′-TCCATCACGGTTTTGGAAT GTTTACTACAC-3′, which corresponds to the luciferase coding region between nucleotide sequence positions 728 and 757, and 5′-GTGCGCCCCCAGAAGC AATTTC-3′, complementary to the luciferase coding region between nucleotide sequence positions 931 and 952. The amount of NP mRNA transcribed from the expression plasmid, which is transcribed by cellular RNA polymerase II, was detected as an internal control.

RESULTS AND DISCUSSION

Stimulation of *de novo* cRNA synthesis by NP. Exogenously added recombinant NP free of RNA (here, designated exogenous NP) stimulated *de novo* virus genome replication in the absence of MCM and any kind of primer (Fig. 1B, lanes 1 to 5). We confirmed by RNase H digestion analyses with primers corresponding to each segment that RNA products corresponded to those synthesized from each segment (data not shown). Then, we examined whether exogenous NP and MCM coordinately stimulate the virus genome replication reaction. MCM stimulated virus genome replication additively with recombinant NP, suggesting that NP and MCM function through distinct mechanisms (Fig. 1B, lanes 6 to 10 and 16 to 20). The stimulatory activity per molecule of MCM was five times higher than that of NP, as judged by the slopes of the lines in Fig. 1C (Fig. 1D). We observed that authentic NP free of RNA purified from virions by CsCl glycerol density gradient centrifugation (5, 34) stimulates activity equally as well as recombi-

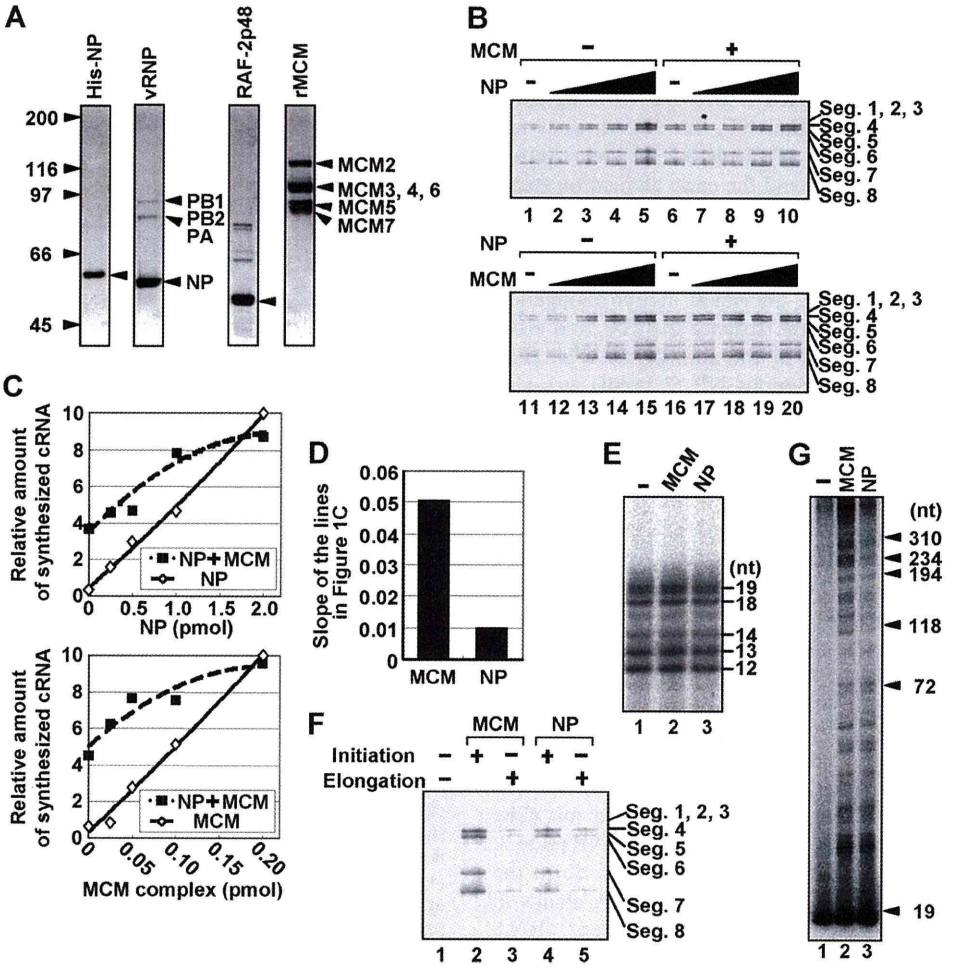

FIG. 1. NP and MCM additively stimulate virus genome replication. (A) Purified recombinant proteins and vRNP. Purified His-NP, vRNP, RAF-2p48/UAP56, and MCM complexes were separated by 7.5% SDS-PAGE and visualized by staining with Coomassie brilliant blue. (B) Stimulatory activity of NP and MCM in cell-free virus genome replication. RNA synthesis was carried out in the absence (lanes 1 to 5) or presence (lanes 6 to 10) of recombinant MCM complex (0.05 pmol of MCM complex) with 0 (lanes 1 and 6), 0.25 (lanes 2 and 7), 0.5 (lanes 3 and 8), 1.0 (lanes 4 and 9), and 2.0 pmol (lanes 5 and 10) of recombinant NP (upper panel). For the experiments shown in the lower panel, we performed the RNA synthesis assay in the absence (lanes 11 to 15) or presence (lanes 16 to 20) of recombinant NP (0.50 pmol) with 0 (lanes 11 and 16), 0.025 (lanes 12 and 17), 0.05 (lanes 13 and 18), 0.10 (lanes 14 and 19), and 0.20 pmol (lanes 15 and 20) of MCM complex (lower panel). (C) Quantitative summary of panel A. The amounts of newly synthesized cRNA corresponding to segment 7 were determined by the ImageJ software. (D) Stimulatory activity per molecule of MCM and NP. The slopes of the lines in the presence of NP or MCM in panel C were determined. (E) Limited elongation assays. Unprimed limited elongation assays were carried out in the absence (lane 1) or presence (lane 2; 0.5 pmol) of MCM or NP (lane 3; 3.0 pmol). (F) NP functions during transition from initiation to elongation reaction. Unprimed limited elongation reactions were performed without (lanes 1, 3, and 5) or with (lanes 2 and 4) either MCM (lane 2; 0.5 pmol) or NP (lane 4; 3.0 pmol). After incubation for 1 h, elongation reactions were restarted by the addition of UTP. For lanes 3 and 5, MCM (0.5 pmol) and NP (3.0 pmol) were added at the restart of elongation reaction, respectively. (G) MCM stimulates the elongation process more effectively than NP. RNA synthesis was carried out in the absence (lane 1) or presence of either MCM (lane 2; 0.5 pmol) or NP (lane 3; 3.0 pmol) with 0.3 μM UTP, 250 μM each ATP, CTP, and GTP, and 10 μCi of [α-^{32}P]UTP (3,000 Ci/mmol). The purified products were separated through 4 to 15% linear gradient PAGE containing 8 M urea and visualized by autoradiography.

nant NP (data not shown). We used as the enzyme source the vRNP containing authentic NP that is bound to the template RNA. Thus, it is quite likely that RNA-free NP but not template-bound NP is required for *de novo* virus genome replication. The RNA synthesis level varied among segments, as previously described (9). For instance, segments 1, 2, and 3 were hardly replicated compared with replication of other segments. The reason for this variation in cRNA synthesis is presently unknown.

NP facilitates the promoter escape of the viral RNA polymerase. Previously, we demonstrated that MCM does not enhance the frequency of replication initiation, but rather makes a nonproductive viral polymerase override the step for abortive synthesis. To examine whether NP is involved in the initiation reaction of virus genome synthesis, we carried out a limited elongation assay, in which UTP is omitted from the reaction mixture and the RNA polymerase pauses at the first adenine residue on the template. The expected lengths of limited elon-

gation products are 12 nt for segments 1, 3, and 7, 13 nt for segments 5 and 8, 14 nt for segment 6, 18 nt for segment 4, and 19 nt for segment 2. Since we detected comparable amounts of each RNA product in the absence or presence of exogenous NP (Fig. 1E), it is concluded that NP, like MCM, does not stimulate the initiation reaction (9). Thus, NP may be required for a step(s) after the initiation and the early elongation steps, in which short cRNAs are synthesized.

To examine whether NP stimulates the transition of the viral polymerase from initiation to elongation, that is, the promoter escape of the viral polymerase, unprimed limited elongation assays were first performed in the absence of UTP, and elongation reactions were restarted by the addition of UTP (Fig. 1F). MCM (0.5 pmol) or exogenous NP (3 pmol) was also added either before or after the limited elongation. The full-length cRNA was synthesized by restarting the limited elongation reaction performed in the presence of MCM (lane 2) or exogenous NP (lane 4) during the limited elongation reaction. Thus, it is quite likely that, to avoid abortive RNA synthesis by the viral polymerase, MCM and NP are required for the viral polymerase prior to its movement along a 12- to 19-nt-long vRNA template from the 3′ terminus of vRNA, where the hairpin loop and double-stranded promoter region are located. Since the initiation reaction was not stimulated by NP (Fig. 1E) and since the viral polymerase could not transit from initiation to elongation in the absence of NP (Fig. 1F), it is possible that NP stimulates elongation complexes during the promoter escape of the viral polymerase, as does MCM (9). A cell-free virus genome replication reaction was also carried out (Fig. 1G) in the presence of MCM (lane 2; 0.5 pmol) or NP (lane 3; 3 pmol) with a low concentration of UTP to slow down the reaction and synthesize a ladder of nascent cRNA chains in order to examine the length of elongated nascent cRNA chains. We found that comparable amounts of cRNA with a shorter length (~100 nt) are synthesized in the presence of either MCM or NP. In contrast, the amount of longer cRNAs (>100 nt) stimulated by MCM was greater than that stimulated by NP (Fig. 1G, compare lane 2 with lane 3). Therefore, it is quite likely that MCM promotes the elongation process more effectively than NP, possibly due to the weak interaction of exogenously added NP with long nascent cRNA, as described later. Taking these results together, it is strongly suggested that NP, like MCM, stimulates the promoter escape of the viral polymerase. Previous reports showed that the target of MCM is PA (9), whereas that of NP is PB1 and PB2 (1). Therefore, it is possible that the replication stimulation mechanisms of NP and MCM are distinct from each other.

Encapsidation of newly synthesized virus genome by NP. Previously, we proposed that MCM stimulates virus genome replication by acting as a scaffold between nascent cRNA chains and the viral polymerase during the promoter escape of the polymerase (9). Since NP has both RNA and viral polymerase binding activities, it should be speculated that NP, like MCM, also functions as a scaffold between newly synthesized RNA and the viral polymerase. To address this, we tried to pull down the replicated cRNA chains associated with His-tagged MCM or NP using Ni-nitrilotriacetic acid (NTA) resin (Fig. 2A). The cell-free virus genome replication reaction was carried out in the presence of an equal molar amount of MCM (lanes 1 and 3) or NP (lanes 2 and 4) with a low concentration

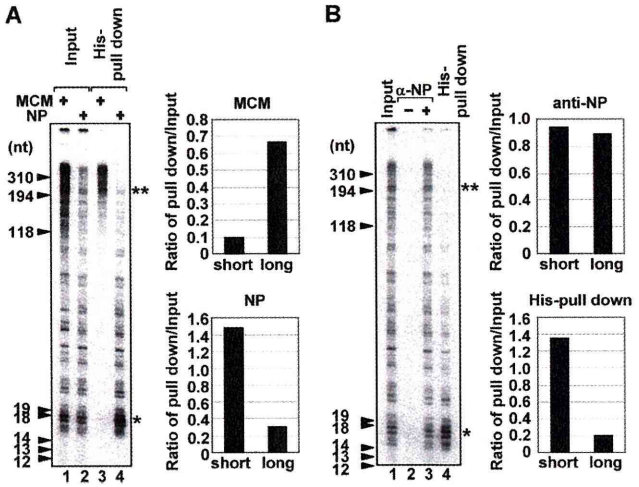

FIG. 2. Encapsidation of nascent cRNA with NP. (A) *De novo* RNA synthesis was carried out in the presence of His-MCM (lanes 1 and 3; 20 pmol) or His-NP (lanes 2 and 4; 20 pmol) with 0.3 μM UTP and 250 μM each ATP, CTP, and GTP and 10 μCi of [α-^{32}P]UTP (3,000 Ci/mmol) in a final volume of 200 μl. The products were purified with His-MCM (lane 3) or His-NP (lane 4) by using Ni-NTA resin. Lanes 1 and 2 represent 20% of the input amounts. The band intensities of short (*) and long (**) nascent cRNA products were quantitatively measured with ImageJ software, and the relative intensity of newly synthesized cRNA coprecipitated with MCM or NP against the input fraction is indicated. (B) *De novo* RNA synthesis was carried out with the authentic vRNP in the presence of His-NP as described for panel A. The newly synthesized RNA products were coimmunoprecipitated without (lane 2) or with (lane 3) anti-NP antibody. Lane 1 shows 20% of the input amount. The product purified by Ni-NTA resin is also represented in lane 4. The band intensities of short (*) and long (**) nascent cRNA products were quantitatively measured with ImageJ software, and the relative intensity of newly synthesized cRNA precipitated by using anti-NP antibody or Ni-NTA resin against input fraction is indicated. α, anti.

of UTP in order to examine the length of copurified RNA as shown in Fig. 1G. As shown in input lanes, MCM stimulated the elongation process more effectively than NP (Fig. 1E and 2A, lanes 1 and 2). Further, longer nascent cRNA chains were preferentially copurified with MCM (Fig. 2A, lane 3), suggesting that MCM stabilizes the elongation complex and thereby makes the viral polymerase escape the promoter successfully. It also seems likely that MCM has a role in the elongation process, but its precise mechanism is still unknown. In contrast, rather shorter cRNA chains were associated with exogenous NP (lane 4). After or along with virus genome replication, the newly synthesized virus genome has to be encapsidated by exogenous NP to form RNP complexes as templates for the next phase of virus genome replication and to protect the virus genome from degradation by cellular nucleases (33). It is hypothesized that encapsidation proceeds by targeting exogenous NP to the nascent RNA through the interaction between NP and the viral polymerase bound to the 5′ end of the nascent RNA to allow NP to interact with the viral RNA preferentially with respect to other cellular RNA species (1, 8, 11, 22), and then subsequently NP is recruited through NP-NP oligomerization (3, 23). In our cell-free system, we found that exogenous NP interacts with shorter cRNA (Fig. 2A, lane 4) without the addition of soluble viral polymerases, which could bind to

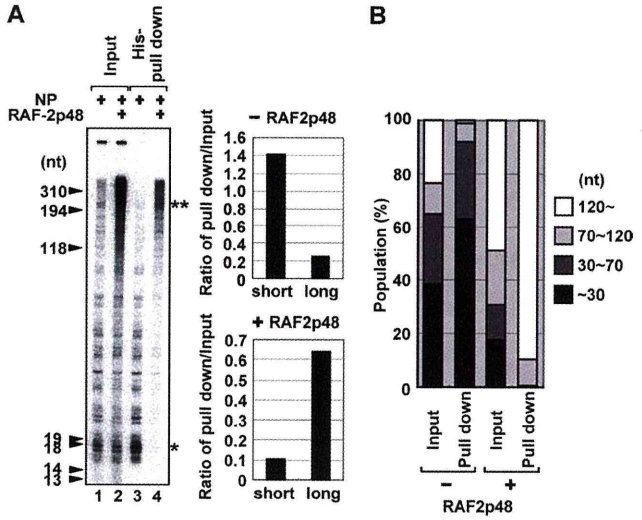

FIG. 3. The stimulatory activity of RAF-2p48/UAP56 in encapsidation of nascent cRNA. (A) RNA synthesis was performed in the absence (lanes 1 and 3) or presence (lanes 2 and 4) of recombinant RAF-2p48/UAP56 with His-NP as described in the legend of Fig. 2. The products were purified with His-NP by using Ni-NTA resin (lanes 3 and 4). Twenty percent of the input amounts is shown in lanes 1 and 2. The band intensities of short (*) and long (**) nascent cRNA products were quantitatively measured with ImageJ software, and the relative intensity of cRNA coprecipitated with NP in the absence or presence of RAF-2p48 against input fraction is indicated. (B) The band intensities of the regions corresponding to RNAs of less than 30 nt, 30 to 70 nt, 70 to 120 nt, and more than 120 nt in each lane in panel A were quantitatively measured with ImageJ software, and the results are indicated as a percentage of the total intensity of each lane.

the 5′ end of the nascent RNA and be a target of NP. It might be explained that the primary targeting of NP to the nascent RNA easily occurs since there is no RNA target other than the nascent RNA in our system. However, it is worth noting that encapsidation of longer nascent cRNA by NP was not achieved when NP was simply added to the system (lane 4). This raises a question of how the newly synthesized virus genome is encapsidated with NP free of RNA.

NP recognizes the phosphodiester backbone of ssRNA in a specific sequence-independent manner. We used, as the enzyme source, the vRNP containing authentic NP, which is bound to the template RNA. Thus, it is reasonably hypothesized that newly synthesized cRNA chains remain associated with the template RNP, possibly by partial hybridization of the nascent cRNA with template vRNA and/or the interaction of nascent cRNA with template-bound authentic NP instead of exogenous NP. To address this, we immunopurified the template-bound authentic NP of vRNP in the presence of exogenous His-NP using anti-NP antibody (Fig. 2B). The length of RNA products associated with authentic NP or both authentic NP and exogenous His-NP (lane 3) was clearly distinct from that of RNA products interacting with only exogenous His-NP (lane 4). From these results, it is assumed that the nascent cRNA product is hardly encapsidated with exogenous NP since the nascent cRNA tends to interact more with template-bound NP than exogenous NP and might partially hybridize with the template.

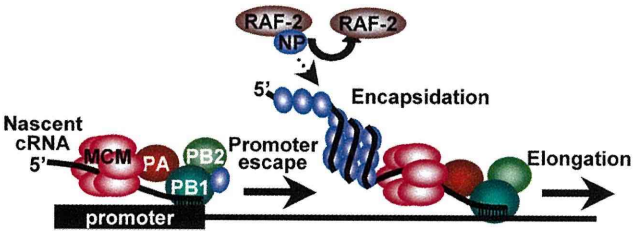

FIG. 4. Proposed model. NP facilitates the promoter escaping from the viral polymerase through the interaction between NP and the viral polymerase in an RNA binding activity-independent manner. During elongation step, RAF-2p48/UAP56 stimulates the coreplicational encapsidation of newly synthesized cRNA with exogenous NP, thereby increasing the processivity of the viral polymerase.

Encapsidation with NP mediated by RAF-2p48/UAP56. As shown in Fig. 2, it is assumed that some factor(s) may be missing in the encapsidation of nascent cRNA products with exogenous NP. Previously, RAF-2p48/UAP56/BAT1 (here, designated RAF-2p48/UAP56) belonging to the DExD-box family of ATP-dependent RNA helicase (13), also reported as NPI-5 (20), was identified as a host factor that binds to NP and stimulates influenza virus RNA synthesis from exogenously added model vRNA templates (16) and that is involved in splicing of cellular pre-mRNAs and messenger RNP maturation of cellular and viral transcripts (4, 25, 29). RAF-2p48/UAP56 binds to NP free of RNA but not to an NP-RNA complex and facilitates NP-RNA complex formation as a molecular chaperone for NP. Therefore, it was proposed that RAF-2p48/UAP56 is involved in the arrangement of NP on the template. However, its precise roles, including the requirement for the encapsidation process, have not yet been uncovered. Thus, we tried to examine whether RAF-2p48/UAP56 facilitates the encapsidation of newly synthesized RNA with exogenous NP (Fig. 3A). We found that long nascent cRNA was encapsidated with exogenous NP by the addition of RAF-2p48/UAP56 (Fig. 3A, compare lane 4, in which RAF-2p48/UAP56 is present, with lane 3, in which RAF-2p48/UAP56 is absent). The ATP-dependent RNA unwinding activity of RAF-2p48/UAP56 was not required for the encapsidation of nascent chains since the encapsidation occurred in the presence of ATPγS, which is a nonhydrolyzable analog of ATP (data not shown). Therefore, we propose a model whereby RAF-2p48/UAP56 facilitates the formation of RNP complexes by coreplicationally transferring exogenous NP to the nascent cRNA chain. It is unlikely that RAF-2p48/UAP56 remodels secondary structures of template and newly synthesized cRNA by its potential RNA helicase activity (Fig. 4). Furthermore, RAF-2p48/UAP56 stimulated the elongation activity of the viral polymerase, possibly by facilitating the encapsidation of nascent cRNA (Fig. 3, lane 2). It is speculated that the coreplicational encapsidation of nascent cRNA by NP may prevent the premature termination of RNA synthesis by avoiding a secondary structure of nascent RNA, which is hypothesized to be one of the causative factors in the termination process of other RNA polymerases (10, 27). Therefore, it is possible that the encapsidation of the nascent RNA with exogenous NP mediated by RAF-2p48/UAP56 increases the processivity of the

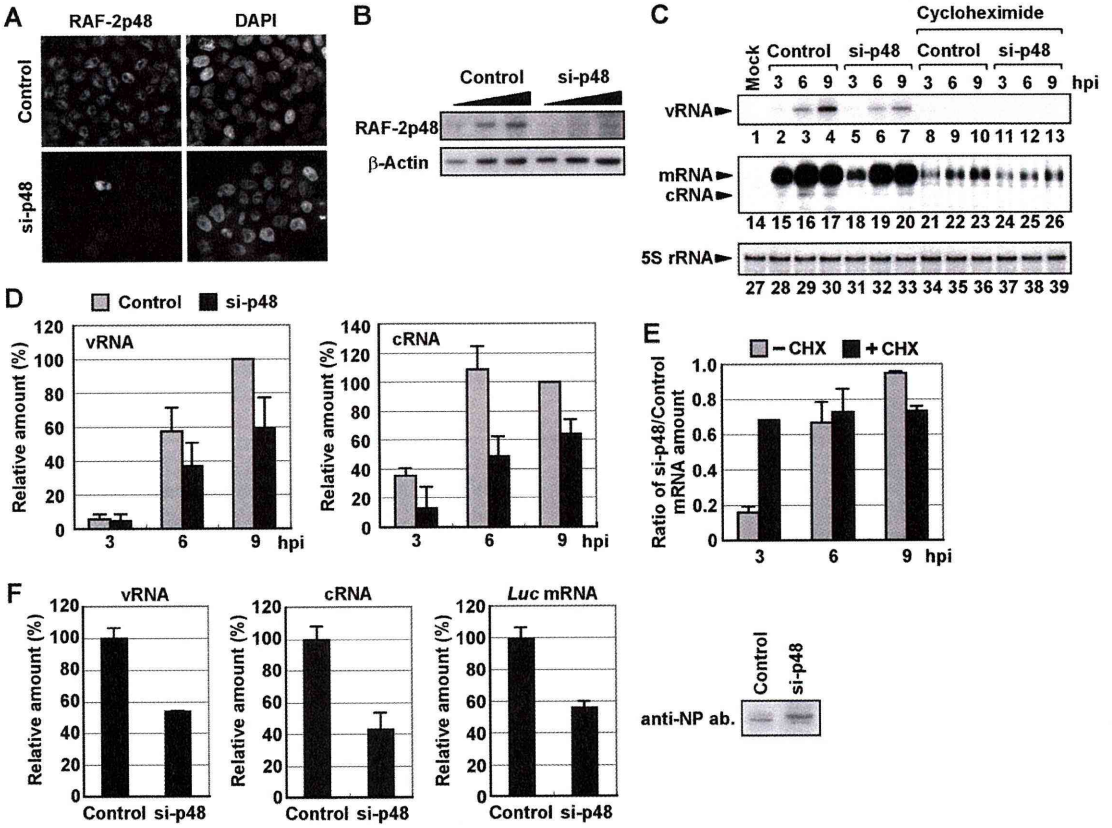

FIG. 5. Involvement of RAF-2p48/UAP56 in influenza virus genome replication in infected cells. (A) At 48 h posttransfection, cells transfected with either a control or siRNA against the RAF-2p48/UAP56 ORF (si-p48) were subjected to indirect immunofluorescence assay with anti-RAF-2p48/UAP56 antibody. Nuclear DNA stained with 4′,6-diamidino-2-phenylindole (DAPI) is also shown. Images were acquired under the same exposure time by a fluorescence microscope system (Axiovision; Carl Zeiss). (B) Expression level of RAF-2p48/UAP56. The lysates prepared from control and RAF-2p48/UAP56 knockdown cells (5×10^3, 1×10^4, and 2×10^4 cells) were separated by SDS-PAGE and then visualized by Western blotting assays with anti-NP and β-actin antibodies. (C, D, and E) Level of viral RNAs in infected RAF-2p48/UAP56 knockdown cells. Control and RAF-2p48/UAP56 knockdown cells were infected with influenza virus in the absence (lanes 1 to 7 and 14 to 20) or presence of cycloheximide (lanes 7 to 13 and 21 to 26) for 0, 3, 6, and 9 h. Primer extension assays were carried out with primers specific for segment 5 vRNA or m/cRNA as described in Materials and Methods. As a loading control, 5S rRNA was also detected (lanes 27 to 39). The band intensities were quantitatively measured by ImageJ software, and the results of three independent experiments are summarized in panel D and are indicated in panel E as the ratio of the mRNA amount in RAF-2p48/UAP56 knockdown cells to that in control cells with or without CHX. (F) The level of viral RNAs synthesized from a reconstituted model replicon in RAF-2p48/UAP56 knockdown cells. Control and RAF-2p48/UAP56 knockdown cells were transfected with plasmids expressing PB1, PB2, PA, and NP and model vRNA encoding the luciferase gene as described in Materials and Methods. At 12 h posttransfection, total RNAs were purified and then subjected to reverse transcription, followed by quantitative real-time PCR with primer sets specific for vRNA, cRNA, and luciferase mRNA. The expression level of NP protein in control and RAF-2p48/UAP56 knockdown cells was also detected by a Western blotting assay with anti-NP antibody (ab).

viral polymerase by avoiding inappropriate secondary structures of nascent cRNA.

Involvement of RAF-2p48/UAP56 in influenza virus genome replication in infected cells. Finally, we tried to examine whether RAF-2p48/UAP56 functions in influenza virus genome replication in cultured cells using siRNA-mediated gene silencing. At 48 h posttransfection of siRNA corresponding to the RAF-2p48/UAP56 ORF, the expression level of RAF-2p48/UAP56 in knockdown cells decreased to approximately 30% of that of cells transfected with the nontargeting siRNA used as a negative control (Fig. 5A and B). We carried out quantitative primer extension assays with appropriate primers specific for each vRNA and mRNA/cRNA of segment 5 (Fig. 5C and D). We confirmed that the product corresponding to cRNA was not found from a fraction bound with oligo(dT) cellulose (data not shown). This result showed that the accumulation of vRNA and cRNA was reduced and delayed in RAF-2p48/UAP56 knockdown cells compared with levels in control cells (Fig. 5C, lanes 1 to 7 and 14 to 20, and D). The same results were obtained for other segments (data not shown). It is proposed that nascent cRNA is degraded unless it is encapsidated with viral RNA polymerase and NP (33). In addition, the results shown in Fig. 3 and a previous report (16) demonstrated that RAF-2p48/UAP56 stimulates the viral polymerase activity. Thus, RAF-2p48/UAP56 might be involved in virus genome replication and encapsidation in infected cells. We also found that the level of NP mRNA in RAF-2p48/UAP56 knockdown cells decreased to 15% in control cells at 3 hpi (Fig. 5C, lanes 15 and 18, and E). In contrast, comparable amounts of NP mRNA were found in both control and RAF-

2p48/UAP56 knockdown cells at 6 and 9 hpi (Fig. 5C, lanes 16, 17, 19, and 20) since the amount of vRNA template sufficient for viral mRNA synthesis might be accumulated at 6 and 9 hpi, but the replication activity was reduced and delayed in RAF-2p48/UAP56 knockdown cells. To confirm the effect of RAF-2p48/UAP56 on viral transcription, we utilized cycloheximide (CHX), a potent protein synthesis inhibitor (Fig. 5C, lanes 8 to 13 and 21 to 26, and E). A previous report showed that CHX suppresses viral protein synthesis and thereby leads to degradation of replicated viral RNA but not mRNA since new vRNP formation was repressed (33). Therefore, we could examine the amount of viral mRNA synthesized from incoming vRNP independent of the level of vRNA accumulation in the presence of CHX (Fig. 5C, lanes 8 to 13, and E). The level of NP mRNA in RAF-2p48/UAP56 knockdown cells was reduced to 70% in control cells in the presence of CHX at 3 hpi (Fig. 5C, lanes 21 and 24, and E). Therefore, it is likely that the reduction of viral mRNA synthesis in RAF-2p48/UAP56 knockdown cells is mainly due to the decrease of vRNP accumulation in the absence of CHX although RAF-2p48/UAP56 has a stimulatory role in viral transcription, possibly by arrangement of NP on template and/or the nuclear export-competent messenger RNP formation (25). To rule out the possibility that the reduction of vRNA and cRNA synthesis was caused by the reduction of viral protein synthesis, we carried out a viral model replicon assay (19, 30) in which active vRNP complexes were reconstituted with PB1, PB2, PA, and NP and the model vRNA encoding the luciferase gene, as described in Materials and Methods (Fig. 5F). With this system, we could examine the viral polymerase activity independent of the expression level of viral proteins since viral proteins were expressed from plasmids under the control of cellular RNA polymerase II promoter in this assay. Results shown in Fig. 5F indicate that vRNA, cRNA, and viral mRNA synthesis was decreased in RAF-2p48/UAP56 knockdown cells compared with that in control cells even in the presence of comparable amounts of NP in both cells. We found that NP synthesized in RAF-2p48/UAP56 knockdown cells migrates differently from that in control cells (Fig. 5F). Previous reports showed that NP is modified by phosphorylation (23) and that its N-terminal region is digested by caspase (35), but the involvement of RAF-2p48/UAP56 in these is not known at present.

It is well known that NP is one of proteins responsible for virus genome replication (15, 18, 27, 33). Recently, it is reported that ubiquitination of NP regulates virus genome replication (12). It is proposed that the soluble viral polymerase might act as a replicative enzyme in *trans*, but transcription occurs from template-bound viral polymerase in *cis* (8). In this study and recent reports (9, 31–33), *de novo* cRNA synthesis is found from template-bound viral polymerase; thus, it could be explained that the soluble viral polymerase might have stimulatory activity but is not completely essential for the synthesis of nascent cRNA. The viral nuclear export protein (NEP/NS2) is also involved in the accumulation level of vRNA and cRNA (26). Further, it is reported that small noncoding RNAs derived from the influenza virus genome might regulate viral transcription and replication through their interaction with viral polymerase complexes (21). To further understand the mechanism of influenza viral genome replication, precise analyses of a functional replicative enzyme including viral and cellular factors are required.

ACKNOWLEDGMENTS

We thank Y. Ishimi (Ibaraki University) for the generous gifts of baculoviruses expressing MCM proteins. This research was supported in part by a grant-in-aid from the Ministry of Education, Culture, Sports, Science, and Technology of Japan (to K.N. and F.M.) and Research Fellowships of the Japanese Society for the Promotion of Science (to A.K.).

REFERENCES

1. **Biswas, S. K., P. L. Boutz, and D. P. Nayak.** 1998. Influenza virus nucleoprotein interacts with influenza virus polymerase proteins. J. Virol. **72:**5493–5501.
2. **Blumberg, B. M., M. Leppert, and D. Kolakofsky.** 1981. Interaction of VSV leader RNA and nucleocapsid protein may control VSV genome replication. Cell **23:**837–845.
3. **Chan, W. H., et al.** 2010. Functional analysis of the influenza virus H5N1 nucleoprotein tail loop reveals amino acids that are crucial for oligomerization and ribonucleoprotein activities. J. Virol. **84:**7337–7345.
4. **Fleckner, J., M. Zhang, J. Valcarcel, and M. R. Green.** 1997. U2AF65 recruits a novel human DEAD box protein required for the U2 snRNP-branchpoint interaction. Genes Dev. **11:**1864–1872.
5. **Honda, A., et al.** 1990. Purification and molecular structure of RNA polymerase from influenza virus A/PR8. J. Biochem. **107:**624–628.
6. **Honda, A., K. Ueda, K. Nagata, and A. Ishihama.** 1988. RNA polymerase of influenza virus: role of NP in RNA chain elongation. J. Biochem. **104:**1021–1026.
7. **Horikami, S. M., J. Curran, D. Kolakofsky, and S. A. Moyer.** 1992. Complexes of Sendai virus NP-P and P-L proteins are required for defective interfering particle genome replication in vitro. J. Virol. **66:**4901–4908.
8. **Jorba, N., R. Coloma, and J. Ortin.** 2009. Genetic trans-complementation establishes a new model for influenza virus RNA transcription and replication. PLoS Pathog. **5:**e1000462.
9. **Kawaguchi, A., and K. Nagata.** 2007. De novo replication of the influenza virus RNA genome is regulated by DNA replicative helicase, MCM. EMBO J. **26:**4566–4575.
10. **Komissarova, N., J. Becker, S. Solter, M. Kireeva, and M. Kashlev.** 2002. Shortening of RNA:DNA hybrid in the elongation complex of RNA polymerase is a prerequisite for transcription termination. Mol. Cell **10:**1151–1162.
11. **Labadie, K., E. Dos Santos Afonso, M. A. Rameix-Welti, S. van der Werf, and N. Naffakh.** 2007. Host-range determinants on the PB2 protein of influenza A viruses control the interaction between the viral polymerase and nucleoprotein in human cells. Virology **362:**271–282.
12. **Liao, T. L., C. Y. Wu, W. C. Su, K. S. Jeng, and M. M. Lai.** 2010. Ubiquitination and deubiquitination of NP protein regulates influenza A virus RNA replication. EMBO J. **29:**3879–3890.
13. **Linder, P., and F. Stutz.** 2001. mRNA export: travelling with DEAD box proteins. Curr. Biol. **11:**R961–R963.
14. **Masters, P. S., and A. K. Banerjee.** 1988. Complex formation with vesicular stomatitis virus phosphoprotein NS prevents binding of nucleocapsid protein N to nonspecific RNA. J. Virol. **62:**2658–2664.
15. **Medcalf, L., E. Poole, D. Elton, and P. Digard.** 1999. Temperature-sensitive lesions in two influenza A viruses defective for replicative transcription disrupt RNA binding by the nucleoprotein. J. Virol. **73:**7349–7356.
16. **Momose, F., et al.** 2001. Cellular splicing factor RAF-2p48/NPI-5/BAT1/UAP56 interacts with the influenza virus nucleoprotein and enhances viral RNA synthesis. J. Virol. **75:**1899–1908.
17. **Nagata, K., A. Kawaguchi, and T. Naito.** 2008. Host factors for replication and transcription of the influenza virus genome. Rev. Med. Virol. **18:**247–260.
18. **Newcomb, L. L., et al.** 2009. Interaction of the influenza a virus nucleocapsid protein with the viral RNA polymerase potentiates unprimed viral RNA replication. J. Virol. **83:**29–36.
19. **Obayashi, E., et al.** 2008. The structural basis for an essential subunit interaction in influenza virus RNA polymerase. Nature **454:**1127–1131.
20. **Palese, P., P. Wang, T. Wolff, and R. E. O'Neill.** 1997. Host-viral protein-protein interactions in influenza virus replication, p. 327–340. *In* M. A. McCrae (ed.), Molecular aspects of host-pathogen interaction. Cambridge University Press, Cambridge, United Kingdom.
21. **Perez, J. T., et al.** 2010. Influenza A virus-generated small RNAs regulate the switch from transcription to replication. Proc. Natl. Acad. Sci. U. S. A. **107:**11525–11530.
22. **Poole, E., D. Elton, L. Medcalf, and P. Digard.** 2004. Functional domains of the influenza A virus PB2 protein: identification of NP- and PB1-binding sites. Virology **321:**120–133.
23. **Portela, A., and P. Digard.** 2002. The influenza virus nucleoprotein: a multifunctional RNA-binding protein pivotal to virus replication. J. Gen. Virol. **83:**723–734.

24. **Qanungo, K. R., D. Shaji, M. Mathur, and A. K. Banerjee.** 2004. Two RNA polymerase complexes from vesicular stomatitis virus-infected cells that carry out transcription and replication of genome RNA. Proc. Natl. Acad. Sci. U. S. A. **101:**5952–5957.
25. **Read, E. K., and P. Digard.** 2010. Individual influenza A virus mRNAs show differential dependence on cellular NXF1/TAP for their nuclear export. J. Gen. Virol. **91:**1290–1301.
26. **Robb, N. C., M. Smith, F. T. Vreede, and E. Fodor.** 2009. NS2/NEP protein regulates transcription and replication of the influenza virus RNA genome. J. Gen. Virol. **90:**1398–1407.
27. **Shapiro, G. I., and R. M. Krug.** 1988. Influenza virus RNA replication in vitro: synthesis of viral template RNAs and virion RNAs in the absence of an added primer. J. Virol. **62:**2285–2290.
28. **Shimizu, K., H. Handa, S. Nakada, and K. Nagata.** 1994. Regulation of influenza virus RNA polymerase activity by cellular and viral factors. Nucleic Acids Res. **22:**5047–5053.
29. **Strasser, K., et al.** 2002. TREX is a conserved complex coupling transcription with messenger RNA export. Nature **417:**304–308.
30. **Sugiyama, K., et al.** 2009. Structural insight into the essential PB1-PB2 subunit contact of the influenza virus RNA polymerase. EMBO J. **28:**1803–1811.
31. **Vreede, F. T., and G. G. Brownlee.** 2007. Influenza virion-derived viral ribonucleoproteins synthesize both mRNA and cRNA in vitro. J. Virol. **81:**2196–2204.
32. **Vreede, F. T., H. Gifford, and G. G. Brownlee.** 2008. Role of initiating nucleoside triphosphate concentrations in the regulation of influenza virus replication and transcription. J. Virol. **82:**6902–6910.
33. **Vreede, F. T., T. E. Jung, and G. G. Brownlee.** 2004. Model suggesting that replication of influenza virus is regulated by stabilization of replicative intermediates. J. Virol. **78:**9568–9572.
34. **Yamanaka, K., A. Ishihama, and K. Nagata.** 1990. Reconstitution of influenza virus RNA-nucleoprotein complexes structurally resembling native viral ribonucleoprotein cores. J. Biol. Chem. **265:**11151–11155.
35. **Zhirnov, O. P., T. E. Konakova, W. Garten, and H. Klenk.** 1999. Caspase-dependent N-terminal cleavage of influenza virus nucleocapsid protein in infected cells. J. Virol. **73:**10158–10163.

Genes to Cells

Synergistic requirement of orphan nonamer-like elements and DNA bending enhanced by HMGB1 for RAG-mediated nicking at cryptic 12-RSS but not authentic 12-RSS

Masashi Numata and Kyosuke Nagata*

Department of Infection Biology, Graduate School of Comprehensive Human Sciences, University of Tsukuba, 1-1-1 Tennodai, Tsukuba 305-8575, Japan

V(D)J recombination is initiated by the specific binding of the recombination activating gene (RAG) complex to the heptamer and nonamer elements within recombination signal sequence (RSS). The break points associated with some chromosomal translocations contain cryptic RSSs, and mistargeting of RAG proteins to these less conserved elements could contribute to an aberrant V(D)J recombination. Recently, we found RAG-dependent recombination in the hotspots of *TEL–AML1* t(12;21)(p13;q22) chromosomal translocation by an extrachromosomal recombination assay. Here, we describe using *in vitro* cleavage assays that RAG proteins directly bind to and introduce nicks into *TEL* and *AML1* translocation regions, which contain several heptamer-like sequences. The cryptic nicking site within the *TEL* fragment was cleaved by RAG proteins essentially depending on a 12-RSS framework, and the nicking activity was enhanced synergistically by both HMGB1 and orphan nonamer-like (NL) sequences, which do not possess counterpart heptamers. In addition, we found that DNA bending stimulated by HMGB1 is indispensable for the HMGB1- and orphan NL element-dependent enhancement of RAG-mediated nicking at the cryptic 12-RSS. Collectively, we would propose the mechanism of HMGB1-dependent enhancement of RAG-mediated nicking at a cryptic RSS through enhanced DNA bending.

Introduction

To produce a huge diversity of lymphocyte antigen receptor in vertebrate, V, D, and J gene segments encoded in germ line arrays are assembled by the process of somatic recombination, known as V(D)J recombination (Tonegawa 1983; Gellert 2002). Each gene segment is flanked by recombination signal sequence (RSS), which consists of highly conserved heptamer element (consensus sequence, 5′-CAC AGTG-3′) and less conserved AT-rich nonamer (consensus sequence, 5′-ACAAAACC-3′). Heptamer and nonamer elements are separated by 12 ± 1 or 23 ± 1 nucleotides, which is known as 12-RSS or 23-RSS, respectively. Recombination activating gene (RAG) 1-RAG2 complex binds to an RSS and introduces a nick at the 5′ side of heptamer, and then a double-strand break (DSB) occurs by transesterification. After introduction of RAG-mediated DSB, the cleaved DNA ends are repaired by nonhomologous end joining (NHEJ) pathway. RAG1 recognizes both heptamer and nonamer sequences, but these elements have distinct roles (Cuomo *et al.* 1996). The heptamer alone can specify an accurate nicking site, and the 5′ three nucleotides (5′-CAC-3′) of the heptamer are highly conserved among RSSs (Hesse *et al.* 1989; Ramsden *et al.* 1994). The nonamer serves a major binding surface for RAG1 (Nagawa *et al.* 1998). The nonamer alone is enough for nick introduction by RAG complex into an appropriate site, but hairpin structure, an intermediate structure of RAG-mediated recombination, is not formed in the absence of the heptamer (Ramsden *et al.* 1996). Normal V(D)J recombination is restricted to immune antigen receptor loci containing authentic RSSs. However, it has been suggested that mistargeting of RAG proteins to cryptic RSSs (cRSSs) might be responsible for

Communicated by: Fumio Hanaoka
**Correspondence*: knagata@md.tsukuba.ac.jp

DOI: 10.1111/j.1365-2443.2011.01534.x

aberrant recombinations other than antigen receptor loci (Kitagawa *et al.* 2002; Marculescu *et al.* 2002; Zhang & Swanson 2008). Indeed, cRSSs are identified in the germ line sequences of *LMO2*, *Ttg-1*, and *HOX11* proto-oncogenes nearby translocation-related break points, especially when antigen receptor loci are fusion partners (Raghavan *et al.* 2001; Zhang & Swanson 2008).

HMGB proteins belong to one of the three classes of high mobility group (HMG) proteins and are relatively abundant architectural nonhistone proteins. HMGB proteins bend DNA, and their DNA bending activity has been thought to enhance the DNA binding and cleavage activity of RAG complex on RSSs, in particular on 23-RSS by enhanced formation of synaptic complex depending on the 12/23 rule of V(D)J recombination (van Gent *et al.* 1997; Sawchuk *et al.* 1997). It has been proposed that HMGB1 facilitates the correct DNA binding and the cleavage activity of RAG proteins at RSSs followed by coordinated DSB depending on the 12/23 rule *in vitro* (Swanson 2002a,b), and simultaneously the addition of HMGB1 represses incorrect RAG-mediated nicking at aberrant sites within the 23-RSS (Yoshida *et al.* 2000). On the contrary, it is recently shown that HMGB1 and HMGB2 can promote the RAG-mediated illegitimate cleavage via the nick/hairpin mechanism (Zhang & Swanson 2009). However, it remains unanswered whether HMGB proteins enhance mistargeting of RAG proteins to cRSSs at the translocation regions identified in lymphoid malignancies.

Recently, it is shown that an aberrant RAG-dependent recombination occurs between *TEL* and *AML1* translocation regions containing several heptamer-like sequences by the extrachromosomal recombination assays (Numata *et al.* 2010). However, the molecular basis of this aberrant RAG-dependent recombination and the involvement of HMGB1 are not clarified fully. For example, it should be investigated whether RAG proteins directly bind to and cleave the cRSSs within *TEL* and *AML1* translocation regions. In addition, it is worthwhile to examine whether HMGB1 enhances the aberrant RAG-mediated cleavage at cryptic sites within *TEL* and *AML1* translocation regions. To address these, we have carried out *in vitro* assays using recombinant RAG and HMGB proteins and *TEL* and *AML1* DNA fragments containing several cryptic sites, which have been characterized by extrachromosomal recombination assays. We found that HMGB1 enhances the direct binding of RAG proteins to the *TEL* and *AML1* translocation regions containing several heptamer-like sequences. Furthermore, the RAG nicking activity at the 12-RSS-like cryptic site was enhanced synergistically by both HMGB1 and orphan nonamer-like (NL) elements, but not at the artificially replaced canonical 12-RSS in the *TEL* translocation locus. Taken these results altogether, it is suggested that RAG proteins contribute to the aberrant DNA nicking step at cRSSs with the aid of HMGB1.

Results

HMGB1 enhances RAG-dependent recombination between *TEL* and *AML1* on a plasmid DNA

It is reported that HMGB1 stimulates RAG-mediated DNA binding and cleavage activity on RSSs in a *cell-free* system (Bergeron *et al.* 2005). However, because it has been unclear whether HMGB1 enhances canonical or aberrant V(D)J recombination *in vivo*, we investigated the effect of HMGB1 on those RAG-dependent recombinations using extrachromosomal recombination assays. 293T cells were transfected with pAT plasmid substrate bearing either 12–23 RSS or *TEL–AML1* translocation regions with full-length human RAG expression vectors in the presence or absence of HMGB1 expression vectors (Numata *et al.* 2010). HMGB1ΔDNA lacking a DNA binding activity was prepared by replacing three hydrophobic residues (Phe 38, Phe 15, and Ile 34) with alanines. The expression levels of HA–RAG proteins and FLAG–HMGB1 proteins were examined by Western blotting with anti-HA and anti-HMGB1 antibodies, respectively (Fig. 1A). HA–RAG1 and 2 were expressed equally in each lane (Fig. 1A, lanes 2–4), and the expression level of exogenous FLAG–HMGB1 protein in each lane was similar to that of endogenous HMGB1 (Fig. 1A, lanes 3 and 4). We found that overexpression of wild-type HMGB1 significantly increased RAG-dependent recombination frequencies on both authentic RSS (Fig. 1B, top panel) and *TEL–AML1* translocation regions (Fig. 1B, bottom panel), whereas HMGB1ΔDNA increased the recombination frequency not significantly enough but slightly. This HMGB1 effect *in vivo* was more for the recombination between *TEL* and *AML1* than for that of authentic RSSs (Fig. 1B).

HMGB1 enhances RAG binding to *TEL* and *AML1* fragments

To examine whether RAG proteins bind to the *TEL* and *AML1* DNA fragments containing the

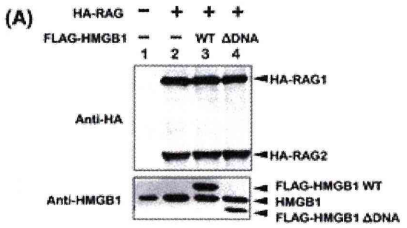

(B)

	AC	ATC	(%) (ATC/AC)x100
Mock	519 000	0	<0.00019
	774 000	0	<0.00013
	672 000	0	<0.00015
RAG	507 000	10 130	1.99802
	566 000	7 000	1.25899
	576 000	8 300	1.44097
RAG +HMGB1	578 000	15 720	2.71972
	668 000	14 900	2.23054
	657 000	16 800	2.55708
RAG +HMGB1 ΔDNA	691 000	14 190	2.05355
	684 000	11 000	1.60819
	754 000	13 900	1.84350

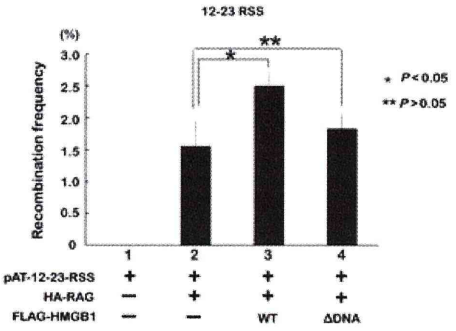

	AC	ATC	(%) (ATC/AC)x100
Mock	358 000	3	0.00084
	654 000	7	0.00107
	660 000	6	0.00091
	131 000	1	0.00076
	113 000	0	<0.00088
RAG	195 000	4	0.00205
	537 000	8	0.00149
	455 000	24	0.00527
	507 000	9	0.00245
	576 000	7	0.00117
RAG +HMGB1	142 000	16	0.01127
	428 000	22	0.00514
	333 000	32	0.00961
	167 000	14	0.00838
	289 000	30	0.01038
RAG +HMGB1 ΔDNA	103 000	7	0.00680
	297 000	6	0.00202
	202 000	16	0.00792
	202 000	6	0.00297
	736 000	15	0.00204

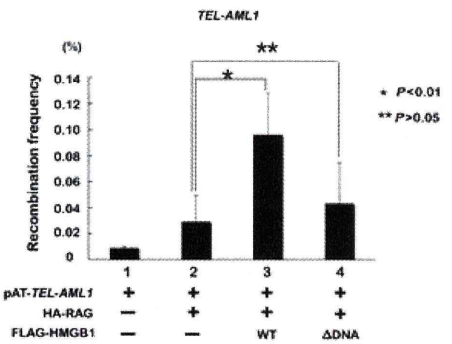

Figure 1 HMGB1 enhances recombination activating gene (RAG)-dependent recombination on pAT-*TEL–AML1* plasmid substrate by an extrachromosomal recombination assay *in vivo*. (A) 293T cells were cotransfected with pAT substrate and expression vectors for HA–RAG proteins and FLAG–HMGB1 proteins. The total cellular proteins were separated through a 10% SDS-PAGE and immunoblotted with anti-HA and anti-HMGB1 antibodies. (B) The tetracycline- and ampicillin-resistant recombinant colonies were counted, and the recombination frequency was calculated as described previously (Numata *et al.* 2010). The recombination assays were repeated three to five times independently.

RAG-dependent recombination sites determined by the extrachromosomal recombination assays (Numata *et al.* 2010), we performed electrophoresis mobility shift assays (EMSAs) using truncated core GST–RAG proteins purified from 293T cells (see Data S1 and Fig. S1 in Supporting Information). As it was indicated in the previous extrachromosomal recombination assays that core RAG proteins cause *TEL–AML1* recombination at the similar level with that of full-length RAG proteins (Numata *et al.* 2010), we used core RAG proteins also *in vitro* assays. For the substrates of EMSAs, we prepared 54-bp-long DNA fragments of *TEL* and *AML1* harboring both the RAG-dependent break points and heptamer-like sequences (Fig. 2A, '*TEL*-1' and '*AML1*-1'). A '12-RSS Mutant' substrate was constructed by replacing heptamer and nonamer consensus sequences in wild-type 12-RSS with the random sequences (Fig. 2A). Only trace amounts of RAG-mediated shifted bands were observed when '12-RSS Mutant' and 'TEL-2'

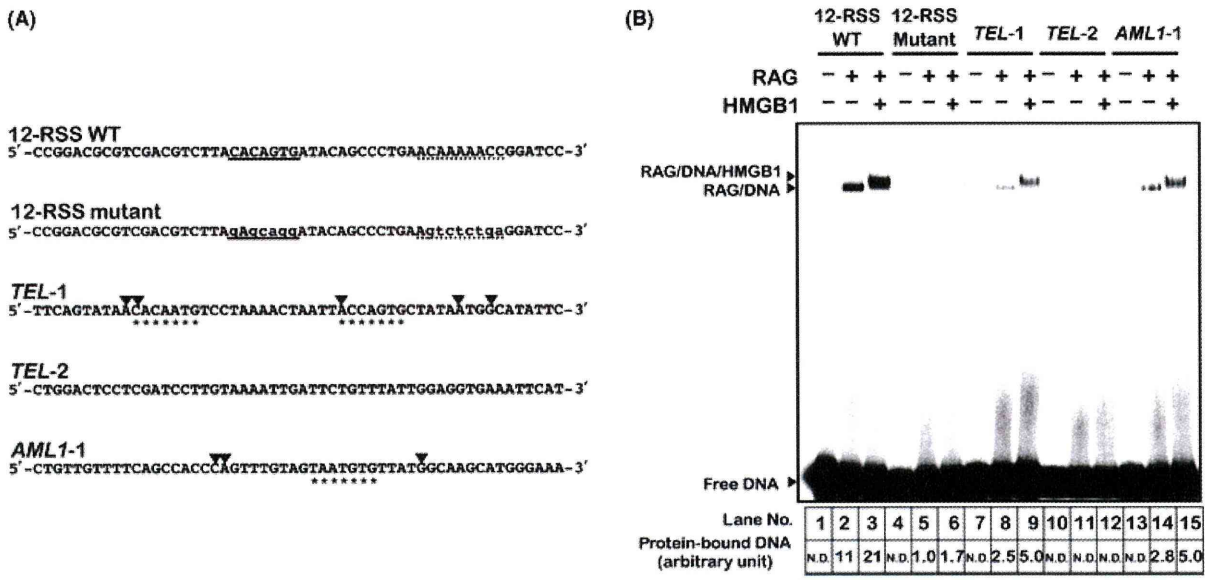

Figure 2 Recombination activating gene (RAG) proteins bind to each *TEL* and *AML1* DNA fragment containing recombination sites. (A) The DNA sequences of top strands of 54-bp-long DNA substrates used in EMSA are indicated. Arrowheads indicate the positions of recombination sites determined previously in the extrachromosomal V(D)J recombination assays (Numata *et al.* 2010). Mutations introduced to heptamer and nonamer sequences are indicated by lower-case letters in '12-recombination signal sequence Mutant' substrate. Underlines and dotted lines indicate heptamer or nonamer sequence, respectively. '*TEL*-1', '*TEL*-2' and '*AML1*-1' were amplified by PCR using sets of primers, TEL-F54 and TEL-R54, TEL-F420 and TEL-R420-54, and AML1-F54 and AML1-R54, respectively. 'Nucleotide sequences with at least 5/7 match to the consensus heptamer element (CAC A/T GTG) are indicated by asterisks. (B) Complex formation of RAG–HMGB1 with DNA substrates. The [^{32}P] end-labeled DNA substrates in panel A were incubated with recombinant proteins (GST-core RAG1 and GST-core RAG2 shown as 'RAG' with or without His-HMGB1 shown as 'HMGB1') as indicated at the top of the gel. Protein–DNA complexes were separated through electrophoresis mobility shift assay, and visualized by autoradiography. The each position of RAG–DNA complex or RAG–HMGB1–DNA complex is indicated on the left side of gel. The experiments were repeated three times independently, and relative amounts of protein-bound DNA are shown below the gel, where the amount in lane 5 is set to be 1. 'N.D.' means 'Not Detected'.

substrates were used. In contrast, RAG proteins bound to each '*TEL*-1' and '*AML1*-1' DNA fragments containing several recombination sites. The effect of HMGB1 was examined in EMSA (Fig. 2B, lanes 3, 6, 9, 12, and 15), because this architectural DNA binding and bending protein is known to enhance the DNA binding and cleavage activity of RAG proteins on authentic RSSs *in vitro* (Aidinis *et al.* 1999). The addition of HMGB1 supershifted RAG–DNA complexes containing '12-RSS', '*TEL*-1', and '*AML1*-1' DNA fragments. Furthermore, HMGB1 enhanced the DNA binding of RAG proteins with these three DNA fragments similarly, by about threefold higher than that in the absence of HMGB1. These results indicate that HMGB1 enhances the RAG binding activity to the *TEL* and *AML1* DNA fragments containing both heptamer-like sequences and RAG-dependent recombination sites.

HMGB1 affects the RAG nicking activity on *TEL* and *AML1* translocation regions

In the course of RAG-mediated recombination, RAG proteins bind to DNA and then introduce a nick juxtapose to the 5′ end of the heptamer sequence of RSS. As the *TEL* and *AML1* fragments containing the RAG-dependent recombination sites were found to possess some heptamer-like sequences, we examined whether RAG proteins introduce nicks *in vitro* around these heptamer-like sequences. To this end, we performed *in vitro* cleavage assays with purified recombinant proteins and the *TEL* and *AML1* DNA fragments, which are [^{32}P] end labeled at the 5′ end of either top or bottom strand. To exclude the possibility that any DNA nuclease activity contaminated in purified RAG proteins generates nicks, we constructed and purified a cleavage-defective mutant of RAG1 (D711A